This paper is currently under review in Science of the Total Environment

How do climate, geomorphology, and land-use control sediment yield generation in an anthropogenically modified landscape?

Sumit Das[1*], Soumi Talukdar[2], Gianvito Scaringi[1]

[1]*Institute of Hydrogeology, Engineering Geology and Applied Geophysics, Charles University, Prague 12800, Czech Republic*

[2]*Department of Physical Geography and Geoecology, Charles University, Prague 12800, Czech Republic*

*For correspondence:

Email: sumit.das@natur.cuni.cz
Mobile: +420 733 637 287
ORCID ID: https://orcid.org/0000-0002-0132-6665

Abstract:

Understanding the controls on sediment yield (SY) is essential for water resource management. However, in the Cauvery basin in India, progress is hindered by fragmented studies that lack an integrated analysis. This research quantifies sub-catchment SY using long-term gauging data and employs Partial Least Squares Regression (PLSR) and multiple regression (MLR) to evaluate geomorphic, climatic, and land-use predictors across 14 representative sub-catchments. Results indicate that geomorphic parameters dominate variation in SY with low hypsometric integral (mean HI = 0.22 ± 0.10), and localised high plan and profile curvature (> 0.01), signifying a mature landscape prone to high sediment export. SY exhibits a strong inverse relationship with the basin area, which reflects significant sediment storage or trapping (dilution effect). Rainfall is the primary climatic driver, while temperature shows no significant link. Land-use effects are secondary and context-dependent, as forests in high-elevation and high-rainfall areas fail to suppress erosion. Crucially, dam infrastructure overrides natural controls by decoupling hillslope erosion from downstream delivery. In fact, the reservoir area alone explains 41% of the SY variability. This study establishes a clear hierarchical relation among the environmental parameters, which is essential for adaptive sediment management, especially targeting headwater erosion hotspots and incorporating sediment continuity into reservoir operations to mitigate downstream impacts.

Keywords: Sediment yield; Geomorphic controls; Anthropogenic impact; Dams; PLSR; Cauvery.

1. Introduction:

An understanding of sediment dynamics in river basins is crucial for comprehending landscape evolution, maintaining ecosystem health, and implementing effective water resource management, which in turn impacts agriculture, hydropower, and biodiversity (Walling & Fang, 2003; Syvitski et al., 2022). Sediment yield (SY) reflects the integrated effects of erosion, transport, and storage processes controlled by geomorphology, climate, and anthropogenic activities (de Vente et al., 2013). In turn, SY influences water quality, reservoir longevity, and agricultural productivity, with profound socio-economic implications (Li et al., 2024). Globally, SYs vary by orders of magnitude, from less than 50 t km^{-2} yr^{-1} in stable lowlands (de Vente et al., 2006; Vanmaercke et al., 2011) to over 5,000 t km^{-2} yr^{-1} in tectonically active high mountains (Lu & Higgitt, 1999; Bhattacharjee et al., 2022).

Rivers worldwide carry ~20 Gt of sediment annually from terrestrial land to the oceans (Milliman & Farnsworth, 2011), but this flux is increasingly disrupted by both natural and anthropogenic drivers. More than 85% of annual rainfall in India occurs between June and September. In many locations, SY exceeds 500 t km^{-2} yr^{-2}, accelerating reservoir siltation and water quality degradation (Das et al., 2021; Jadhav et al., 2024). In India, rapid land-use change, climate intensification, and soil degradation amplify sediment-related risks, including reservoir siltation (Singh et al., 2025), water quality decline (Shukla et al., 2018, Rehana et al., 2012), and loss of arable land (Zhang and Cai, 2011).

The Cauvery, South India's largest and most important catchment, epitomises these challenges. The reservoirs in the basin, including Mettur, Krishnaraja Sagar, and Bhavani, are losing 0.5–1.2% of their storage capacity each year owing to sedimentation, which significantly threatens hydropower generation and irrigation land for ~1300 thousand hectares (CWC, 2014). Meanwhile,

sediment starvation in the delta due to upstream trapping has exacerbated coastal erosion (Das et al. 2025). With climate models projecting an increase of about 4–10% in extreme rainfall by 2060 (Chaubey & Mall, 2023) and ongoing rapid land-use changes (Poyil et al., 2016), understanding the factors controlling SY in the Cauvery has become urgent.

Geomorphology establishes the foundational control on SY by dictating erosion potential and sediment connectivity. Catchment-scale geomorphic characteristics such as slope, relief, drainage density, and hypsometric integral (HI) strongly correlate with SY patterns globally (Zhang et al., 2015). For instance, topographic curvature and HI have been identified as the main geomorphic drivers in the Loess Plateau, accounting for over 60% of the spatial SY variability. (Zhang et al., 2015).

On the other hand, climate, particularly the magnitude and intensity of precipitation, serves as the primary erosive agent. In steep orogens, rainstorms generate significant SYs, both through surface erosion and by triggering landslides on the hillslopes that quickly deliver sediment into the river network (Bookhagen et al. 2005; Yunus et al. 2025). Critically, precipitation often exhibits strong nonlinear interactions with other drivers. In glaciated high mountain basins in Asia, SY is noticeably higher (Himalaya-Karakoram-Hindu Kush: SY ~1000 t km^{-2} yr^{-1}; rainfall ~710 mm yr^{-1}; slope ~19°) in basins with higher mean annual rainfall (Li et al., 2024). Furthermore, studies suggest that temperature exerts a strong control on erosion and sediment distribution in rivers (Hirschberg et al., 2020; Tan et al., 2023).

Land use and vegetation cover introduce further complexity by modifying runoff generation, infiltration, and soil detachment resistance (Nadal-Romero et al., 2025). Agricultural expansion generally increases SYs compared to natural vegetation by reducing ground cover and disrupting soil structure (Donovan & Monaghan, 2021). Notably, vegetation's role can be bidirectional and

context-dependent. For instance, in humid eastern Tibet, SY increased with denser vegetation, attributed to rain-enhanced bio-weathering processes. Conversely, in arid Tien Shan, SY decreased due to effective slope stabilisation by roots (Li et al., 2024). In the wetter environments of the Himalayas, dense vegetation cover resists storm-induced soil erosion (Olen et al. 2016).

Research on the drivers of SY in Indian river basins has advanced recently (Das et al. 2023), but it still remains highly fragmented. Prevailing studies frequently focus on isolated factors and lack robust multivariate statistical frameworks capable of addressing inherent predictor collinearity. These studies frequently depend on geospatial modeling using the Universal Soil Loss Equation (USLE) or Revised Universal Soil Loss Equation (RUSLE) to predict SY (Majhi et al., 2021, Samal et al., 2024). However, these approaches have significant limitations, including limited or no site-specific validation, few local to catchment-scale sediment studies, and insufficient investigation of the complex interactions among geomorphic, climatic, and anthropogenic factors that control spatial SY variability. Notably, no comprehensive large-scale study within India, except the Godavari (Das et al., 2023), has simultaneously integrated geomorphic, climatic, and land-use predictors using advanced statistical techniques.

This gap is particularly significant for the Cauvery basin which is characterized by (a) pronounced geomorphic diversity where steep, highly dissected slopes near the Western Ghats and BR-MM Block Mountain ranges contrast sharply with the low-relief central and lower reaches; (b) strong climatic gradients ranging from extreme rainfall in the humid headwater to semi-arid plateaus; and (c) rapid land use transformation marked by significant decrease in forest cover since recent decades and widespread conversion to agricultural lands, and (d) anthropogenically modified stream with several large multipurpose dams and reservoirs.

Existing studies on SYs in the Cauvery basin (Vaithiyanathan et al., 1992, Hariprasad et al. 2024) have not fully addressed the environmental factors influencing the spatial variability of SY at the catchment scale. Hence, this study aims to fill these gaps with two main objectives: (i) assess sub-basin-scale SY using long-term sediment gauging data, and (ii) determine the main factors controlling the spatial differences in SY within the Cauvery basin.

2. Study area:

2.1. General overview of the catchment:

The Cauvery, one of the most significant rivers in Peninsular India, originates in the Western Ghats at an elevation of 1341 m asl and flows southwest for about 800 km before debouching into the Bay of Bengal (Fig. 1a). Its catchment area is bordered by the Pennar and Tungabhadra basins to the north, the Palar Basin to the south, the Western Ghats to the west, and the Nilgiri Hills extending into the Eastern Ghats to the east. The Cauvery and its 21 tributaries form a dendritic drainage network, with several local areas displaying a semi-box-shaped channel pattern.

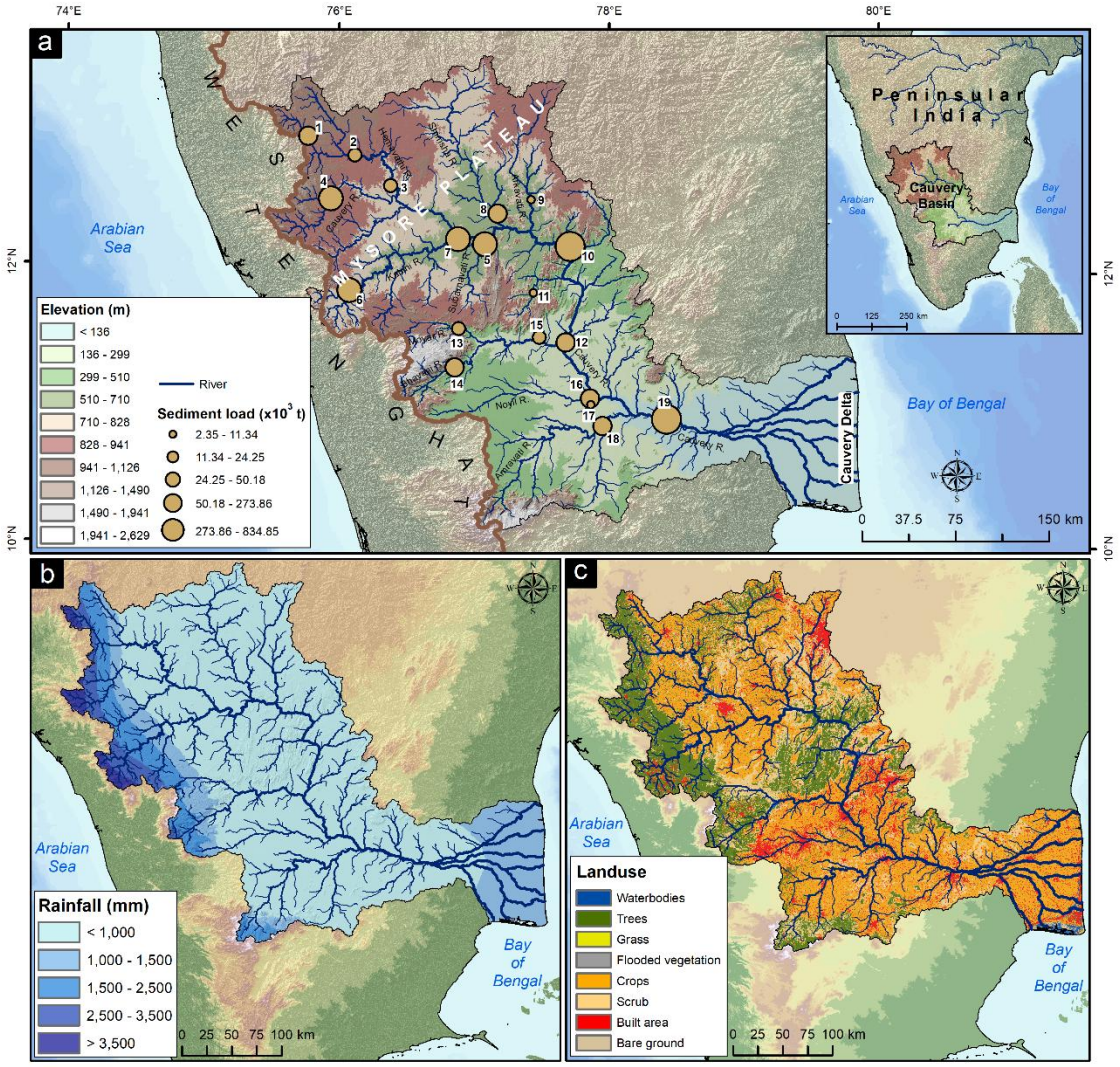

Fig. 1. (a) Overview of the Cauvery Basin, the most important river network in South India. The circles indicate the locations of gauging stations included in this study. Refer to Table 1 for detailed information on the gauging stations. (b) Spatial variation in rainfall: the western part near the Western Ghats receives extremely high rainfall, while the central region is a semi-arid dry zone. (c) Dominant land cover types (Source: Environmental Systems Research Institute [ESRI]).

Geomorphologically, the catchment can be divided into three distinct units: (i) the Mysore Plateau in the west, characterised by higher elevation and subdued relief, (ii) the Tamil Nadu fluvio-deltaic plain in the east, and (iii) the intervening block mountain ranges, including the Nilgiri Hills, Biligirirangan-Mahadeswaramalai (BR-MM) ranges, and Shevaroy Hills in between (Kale et al.,

2014, Chidambaram et al., 2019). The upper and middle segments of the catchment feature escarpments, hanging tributaries, entrenched valleys, canyons, lakes, and waterfalls.

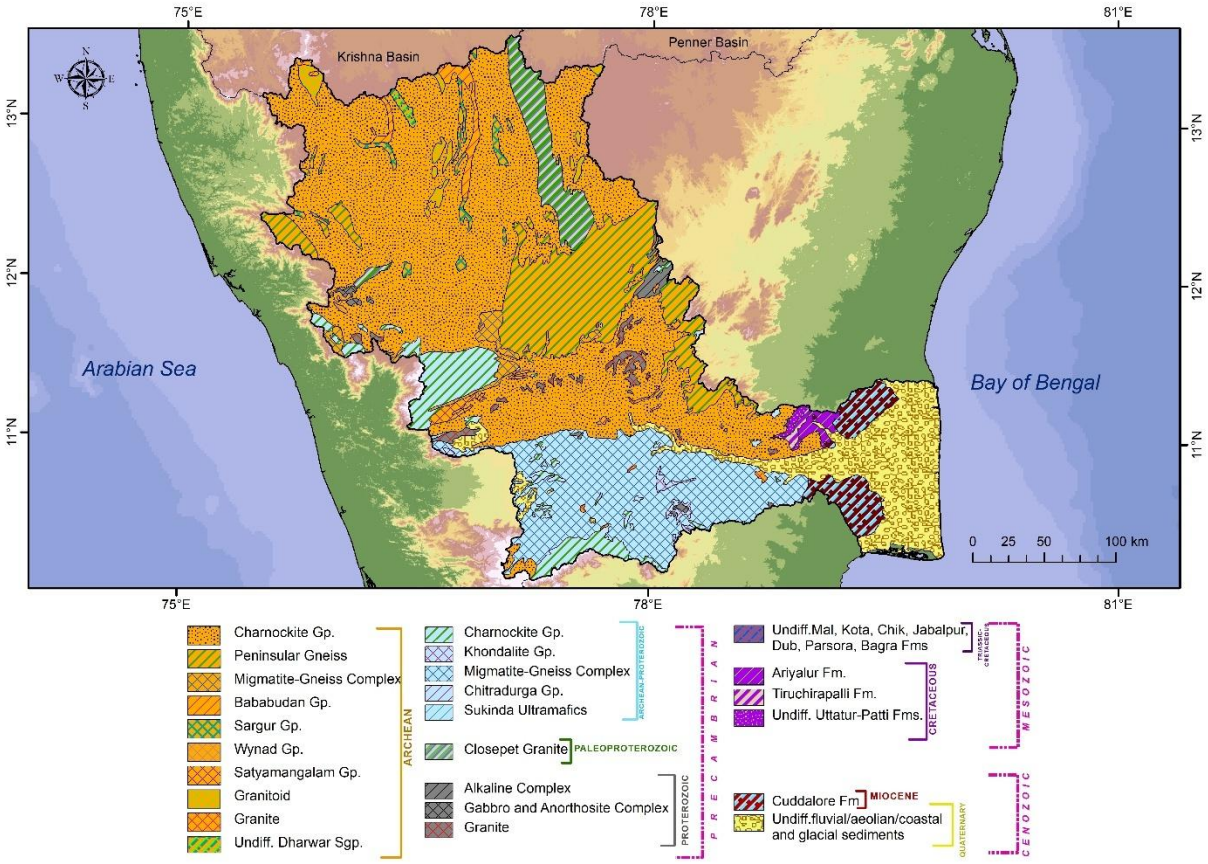

Fig. 2. Lithological variation in the Cauvery basin. The majority of the basin is underlain by Precambrian Charnockite-Gneiss-Granite formation, whereas the deltaic part is covered by Quaternary deposits.

Geologically, the Cauvery Basin is a peri-cratonic rift basin (Chari et al., 1995) formed along the eastern continental passive margin during the late Jurassic-Post Cretaceous period (Twinkle et al., 2016). The upper catchment primarily drains the Dharwar craton, composed of some of the oldest continental basement rocks from the Archean and Proterozoic eons (Fig. 2). The block mountains in the central-lower part of the catchment are part of high-grade Archean to Meso-Neoarchean Granulite of the Southern Granulite Terrain, dissected by a complex set of shear zones (Sajeev,

2021). Several prominent faults and lineaments traverse the central part of the catchment. Fluvio-deltaic sedimentation in the basin is largely of Cretaceous-Tertiary-Quaternary origin.

The climate across the basin ranges from tropical to subtropical monsoonal, with notable spatial variation in precipitation. The source region in the Western Ghats receives over 3,500 mm of annual rainfall during the monsoon season (Fig. 1b). In contrast, the semi-arid valleys of Tamil Nadu and Karnataka receive much lower rainfall. The deltaic tract receives moderate rainfall, mainly during the retreating northeast monsoon between October to December. Temperature variation is minimal in the upland regions but remains high and relatively stable across the delta.

Land use across the catchment is predominantly agricultural and forested, with a smaller extent of rangeland, built-up areas, and waterbodies (Fig 1c). However, land use patterns are undergoing rapid transformation owing to deforestation, agricultural expansion, and rapid urbanisation.

2.2. Sediment transport characteristics:

Several studies have documented a significant drop in sediment flux in the Cauvery River because of sediment trapping by many large-capacity reservoirs (Das, 2021; Gupta et al., 2012). For instance, sediment load measured at Biligundulu station (middle reach = 834 kt/yr) decreased sharply to 50 kt/ yr at Urachikottai, primarily due to sediment retention by the Mettur dam, situated between these two gauging stations (Fig. 3). Consequently, sediment delivery to the deltaic region has significantly declined (Das et al., 2025).

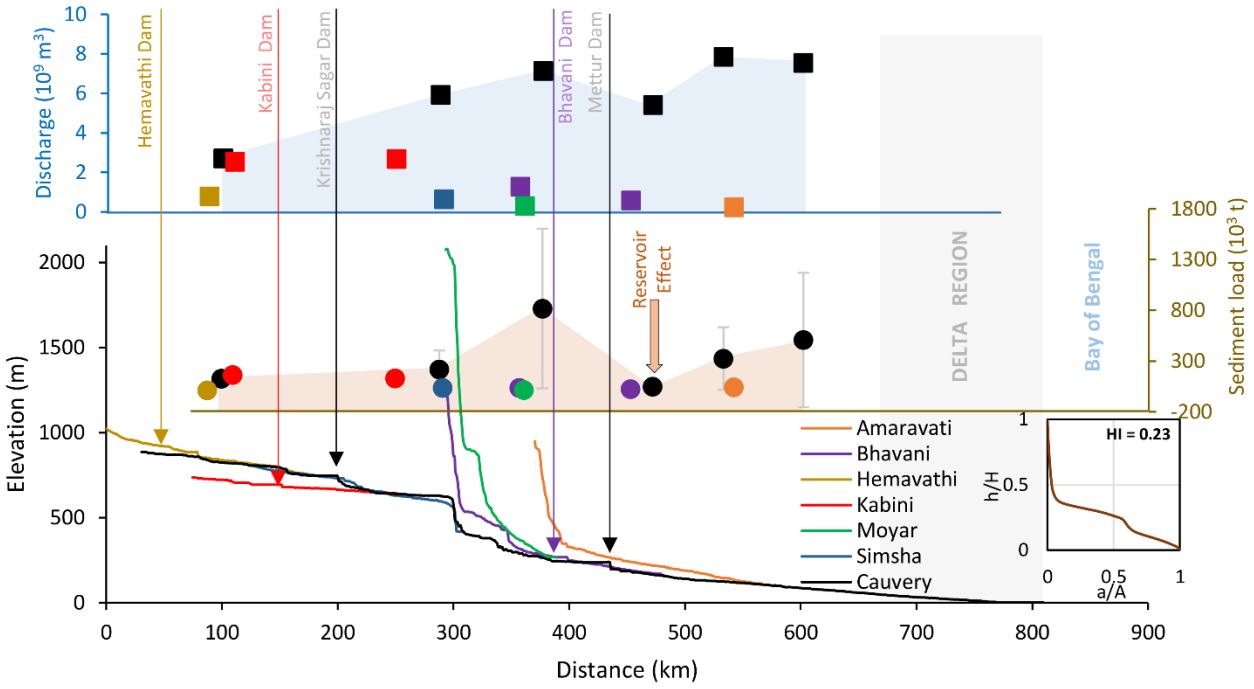

Fig. 3. Composite longitudinal profile of the Cauvery River mainstem and major tributaries. Variations in discharge and sediment load at gauging stations are shown along the main river following the profile. The inset represents the hypsometric curve for the entire catchment. Only the major dams along the main rivers and its tributaries are marked.

The natural hydrological regime of the Cauvery Basin has been significantly altered in recent decades owing to hydroclimatic shifts and human activity. Projected increases in temperature and evapotranspiration are likely to reduce annual runoff despite high rainfall (Gosain et al., 2006). The construction of numerous dams, reservoirs, and barrages has further disrupted the basin's hydrological connectivity and worsened water stress (Gowri et al., 2021; Ekka et al., 2022).

3. Data and methodology:

3.1. Data sources:

This study relied on multiple freely available datasets to analyse the factors influencing sediment dynamics within the Cauvery Basin. Annual sediment load data from 19 gauging stations located across the main channel and various tributaries of the Cauvery River were obtained from the

Central Water Commission (CWC) hydrological yearbook (CWC, 2019a). Although the Cauvery basin has over 25 monitoring gauging stations, 19 stations were selected based on the availability of consistent and complete sediment concentration records (Table 1). The Shuttle Radar Topography Mission (SRTM) Digital Elevation Model (DEM) is globally recognized (Berry et al., 2007) for their uniform quality and broad spatial coverage, making them particularly valuable for terrain analysis. This dataset allows for the seamless extraction of crucial topographic parameters, which are essential for assessing sediment transport potential and catchment-scale erosion modeling.

Climatic parameters were derived from the WorldClim 2.1 dataset of long-term average precipitation and temperature data at a spatial resolution of 30 arcsec. WorldClim provides high-quality interpolated climate data that are extensively used in environmental and hydrological modeling (Hijmans et al., 2005; Panagos et al., 2017).

High-resolution land use data were derived from the Environmental Systems Research Institute (ESRI) land cover layer available via the ArcGIS Living Atlas with 10-m resolution. Geological attributes such as lithology at a scale of 1:2,000,000 and lineament at a scale of 1:250,000 were acquired from the Bhukosh portal of the Geological Survey of India (GSI). Information on dams within the Cauvery Basin was extracted from the National Register of Large Dams (CWC, 2019b).

3.2. Catchment delineation and sediment yield computation:

Using digital topographic data, 19 sub-catchments were delineated based on the location of gauging stations across the Cauvery Basin. These sub-catchments are not traditional hydrological units but represent the unique drainage area in between gauging stations, excluding any overlapping drainage from upstream sites. This approach ensures that sediment yield calculations

207 are spatially independent and reflect localised environmental and geomorphic factors operating
208 within each catchment that uniquely affect its yield (Das et al., 2023).

209 Only 14 of the 19 sub-catchments were included in the statistical analysis. The remaining 5 were
210 excluded because of negative sediment yield values caused by sediment sequestration behind
211 dams, which led to the outflux falling below the influx. Gauging stations within the fluvio-deltaic
212 zone were also excluded to prevent underestimating the sediment yield caused by the distributary
213 channels.

214 The long-term average sediment loads were derived from annual sediment load data to reduce the
215 effects of short-term fluctuations. Each sub-catchment's average sediment load (t yr^{-1}) was
216 calculated based on the upstream contributing area and adjusted for station order along the
217 downstream flow path to avoid redundancy from overlapping inputs. Furthermore, the SY (t km^{-2}
218 yr^{-1}) for each sub-catchment was computed by normalising the average sediment load by the
219 respective sub-catchment area:

220 $$SY = \frac{Q_s^{avg}}{A}$$

221 where Q_s^{avg} is the long-term mean annual sediment load, and A denotes the catchment area.

222 **3.3. Computation of variables:**

223 Geomorphic characterisation of individual sub-catchments was performed by deriving several
224 primary geomorphic parameters such as drainage area, perimeter, total stream length, mean slope,
225 drainage density, form factor, elongation ratio, circularity ratio, total relief, and relief ratio using
226 the SRTM DEM. Subsequently, several other secondary and compound factors related to surface
227 process were calculated, namely HI, plan curvature, profile curvature, Topographic Ruggedness

Index (TRI), Topographic Wetness Index (TWI), and slope-length factor. Power-law scaling between slope and area was used to estimate the steepness index:

$$S = k_s A^{-\theta}$$

where k_s denotes the steepness index and θ indicates concavity. A reference concavity of 0.45 was used to normalise k_{sn} and enable comparisons across catchments. Mean values of these geomorphic parameters for each sub-catchment were further calculated. Structural controls on sediment generation were assessed through lineament density, computed within a 10 km radial buffer and expressed as mean density for each sub-catchment.

Land cover composition, a critical control on erosional processes, was derived from ESRI categorical data. To focus on established primary drivers of land erosion, five primary land cover classes (i.e., tree, crop, range land, built-up areas, and waterbodies) were selected among the ten original land cover categories. For each sub-catchment, the land cover raster was clipped to the watershed boundary, and the proportional areal coverage (%) of each target category was computed.

Gridded precipitation and temperature data for each sub-catchment covered multiple pixels. The average precipitation and temperature across all pixels within each sub-catchment were calculated and used for later statistical analysis.

3.4. Partial least-squares regression (PLSR):

In sediment yield studies, Partial Least-Squares Regression (PLSR) has been widely adopted to address high-dimensional, collinear, and noisy datasets (e.g., Yan et al., 2013; Shi et al., 2014). PLSR is highly appropriate for problems with a number of observations lower than the number of predictors.

In this study, PLSR was employed to identify and quantify the influence of 29 predictor variables on SY across the studied sub-catchments. Given the high predictor-to-observation ratio, which renders ordinary least squares unsuitable owing to multicollinearity and overfitting, PLSR is ideal as it extracts latent variables (components) by maximising the covariance between the predictor matrix "X" and the response vector "Y". The model can be expressed as:

$$X = TP^T + E, \qquad Y = Uq^T + F$$

where T and U are score matrices, P and q are loading vectors, and E and F are residuals. The inner relation linking T and U is:

$$U = TB$$

where B is a diagonal matrix of regression coefficients. The relationship between T and U is assumed to be linear. The regression coefficient matrix in the original space is:

$$B_{PLS} = W(P^T W)^{-1} Q^T$$

where W is the weight matrix.

The model's goodness-of-fit (R^2) and predictive power (Q^2) were assessed using:

$$R^2 = 1 - \frac{\sum(y_i - \hat{y}_i)^2}{\sum(y_i - \bar{y})^2}\ , \qquad Q^2 = 1 - \frac{\sum(y_i - \hat{y}_i, CV)^2}{\sum(y_i - \bar{y})^2}$$

where $\hat{y}_i, CV$ is the predicted value from cross-validation, R^2 reflects calibration fit, and Q^2 derived via leave-one-out CV, indicates predictive reliability (the higher, the better). An optimal balance between the values of Q^2 and R^2 can be achieved by choosing an appropriate number of latent variables or components (Li et al. 2019). Q^2 values above ~0.4–0.5 are deemed acceptable for predictive reliability.

The Variable Importance in Projection (VIP) was computed to determine the relative contribution of each predictor to the underlying variability of the response vector "Y" across all components:

$$VIP_j = \sqrt{p \cdot \frac{\sum_{k=1}^{A} SS_k \left(\frac{w_{jk}^2}{\|w_k\|^2} \right)}{\sum_{k=1}^{A} SS_k}}$$

where p is the number of predictors, A is the number of components, SS_k is the variance in Y explained by component k, w_{jk} is the weight of predictor j on component k, and $\|w_k\|$ is the norm of the weight vector. Predictors with VIP > 1.0 were considered highly significant for influencing the SY variation in the Cauvery Basin.

With 29 predictors and only 14 observations, PLSR reduces overfitting by projecting predictors and response variables into a smaller set of latent variables. PLSR's primary advantages are its ability to handle multicollinearity (Wold et al., 2001) and provide interpretable latent structures. However, disadvantages include sensitivity to outliers and subjective component selection (Abdi, 2010). For this study, R^2 and Q^2 were evaluated to ensure model reliability, while VIP was used to prioritize key factors amid dimensionality challenges. The XLSTAT software package was used to compute statistics.

3.5. Multiple Linear regression (MLR):

To complement the PLSR analysis and provide a benchmark for linear modeling, Multiple Linear Regression (MLR) was also conducted. For MLR, the variables were grouped based on their characteristics (e.g., geomorphic, climatic, land use), and several common combinations exerting a coupled effect on SY variability were inspected to evaluate the explained variance (R^2) for the SY distribution.

4. Results:

4.1. Sub-catchment specific sediment load and yield:

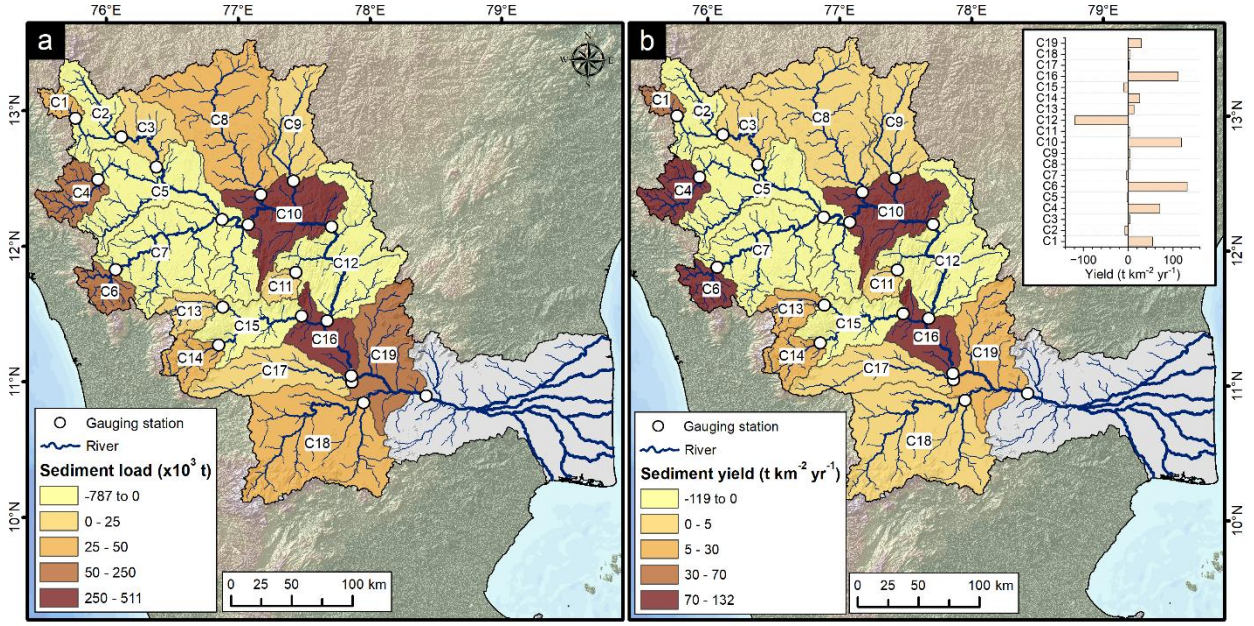

Fig. 4. (a) Variation in sediment load across 14 sub-catchments in the Cauvery Basin, and (b) variation in sediment yield.

Sediment load and SY exhibit pronounced heterogeneity across the 19 sub-catchments of the Cauvery Basin (Fig. 4a). The highest sediment load occurs at sub-catchment C10 (511 kt yr^{-1}), followed by C16 (257 kt yr^{-1}), both situated within the BR-MM hills. In contrast, the lowest loads are observed in C3 (8 kt yr^{-1}), C11 (2 kt yr^{-1}), and C17 (7 kt yr^{-1}). C19, the sub-catchment representing the terminal gauging station, shows a lower load (138 kt yr^{-1}) than several upstream sub-catchments. Five sub-catchments (C2, C5, C7, C12, and C15) exhibit negative sediment loads, reflecting substantial net sediment deposition within reservoirs where upstream sediment input exceeds outflow.

The SY, calculated by area normalisation, displays distinct spatial patterns (Fig. 4b), ranging from 2 t km^{-2} yr^{-1} (C17) to 132 t km^{-2} yr^{-1} (C6). Moderate to high SY values (mean = 59 ± 42 t km^{-2} yr^{-}

306 [1]) characterise sub-catchments adjacent to the Western Ghats and the hilly Mysore plateau, while
307 the lowest SY occurs in the foothills of the BR-MM hills.

308 Catchment size strongly influences SYs. The largest sub-catchment (C8: 8106 km^2) yields only 5
309 t km^{-2} yr^{-1}, whereas the smallest (C1: 592 km^2) yields 55 t km^{-2} yr^{-1}. Sub-catchments with the
310 highest yields (C6: 132 t km^{-2} yr^{-1}; C10: 119 t km^{-2} yr^{-1}; C4: 71 t km^{-2} yr^{-1}) have moderate drainage
311 areas (1258 km^2, 4303 km^2 and 1757 km^2, respectively). Sub-catchments with negative SY were
312 excluded from statistical analysis.

313 SY across all the sub-catchments (excluding those with negative SY) shows a very high coefficient
314 of variation (CV = 111%). This variability reflects the study area's complex topographic
315 heterogeneity, strong rainfall gradients, diverse land use, and differential hydro-morphological
316 alteration from anthropogenic activities.

317 4.2. Variation in factors influencing sediment yield:

318 Substantial geomorphic, climate, and land use diversity characterise the 14 sub-catchments of the
319 Cauvery Basin analysed in this study (Table 2). Key morphometric parameters show wide ranges.
320 The basin perimeter ranges from 149 km (C1) to 546 km (C8), with an average of 321 km. Stream
321 length is maximum and minimum in C18 (2316 km) and C1 (148 km), respectively. Relief varies
322 from 418 (C3) to 2394 (C18). Dominantly high elongation ratios (> 0.50) reveal a prevalent semi-
323 circular to circular sub-catchment form. The basin-wide mean hypsometric integral (0.22 ± 0.10)
324 values, ranging from 0.08 (C16) to 0.40 (C13), collectively point to a mature erosional stage.
325 Steeper slopes correlate with the sub-catchment's proximity to the Western Ghats escarpment,
326 varying from 2° (C8, C16) to 14° (C14). This is reflected in the high TRI values (mean 7.43 ±
327 4.67; 2.62–18.03) and variable TWI (7.48–10.02). The normalised steepness index (k_{sn}) varies

from 6 (C6) to 107 (C13). Significant contrasts in k_{sn} (6–107), indicative of transient drainage adjustment and concentrated near knickpoints, further indicate basin heterogeneity. High coefficients of variation (CV > 50%) for most variables (A, SL, E_{min}, R_r, S, LS, C_{plan}, C_{pro}, TRI, k_{sn}) confirm this spatial variability, with drainage density (D_d) being the notable exception (CV < 10%) (Fig. 5).

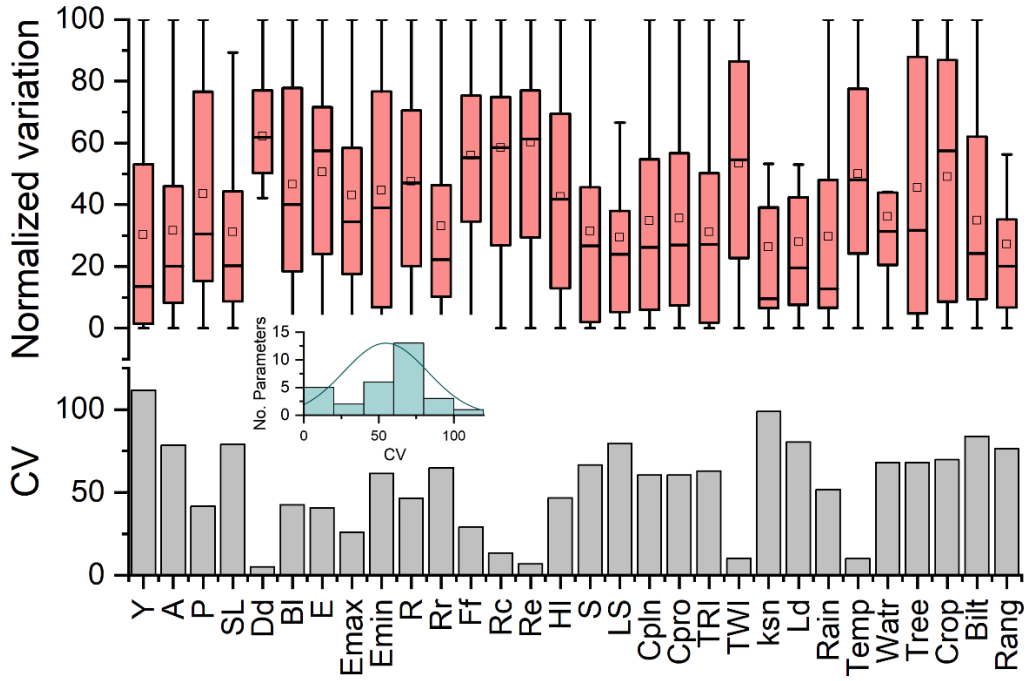

Fig. 5. Normalised distributions and coefficients of variation for all the computed parameters in the studied sub-catchments. High variability (CV > 50%) is observed in more than 15 parameters.

Climatic variables exhibit substantial spatial heterogeneity across the basin. Precipitation depends on the orographic gradient, ranging from 661 mm (C3, leeward) to 2662 mm (C6, windward). The westernmost sub-catchments receive moisture from the summer monsoon, while the downstream reaches are influenced primarily by the retreating (winter) monsoon. Mean annual temperature averages 24.0 ± 2.4°C basin-wide but reflects elevation contrasts; maxima occur near the delta (C19: 28°C), contrasting with minima in the elevated Western Ghats (C13: 20°C).

Land use is predominantly arboreal and agricultural. Tree cover is spatially diverse (sub-catchment mean: 41 ± 28%), exceeding 50% in six sub-catchments (C1, C4, C6, C11, C13, C14) but falling below 10% in three (C9, C16, C17). Conversely, cropland coverage exceeds 50% in five sub-catchments and falls below 10% in five others, peaking in C16 (63%), coincident with high sediment yield (SY), and reaching a minimum in C1 (4%). Rangeland (shrub/scrub/barren) is typically limited and covers <10% area in most sub-catchments, except C13 (40%). Built-up areas (mean 11%) and water bodies (mean 1%) represent negligible land cover components.

4.3. PLSR in explaining influences:

A preliminary Pearson correlation analysis reveals significant multicollinearity ($p < 0.05$) among geomorphic, climatic, and land-use parameters across the sub-catchments (Fig. 6). Strong pairwise interdependencies are observed within geomorphic variables, including basin morphometrics (perimeter, length, mean elevation) and terrain derivatives (slope, LS factor, TRI, TWI, plan and profile curvatures). Climatic parameters exhibit significant covariation between rainfall and temperature. Likewise, land-use compositions demonstrate significant correlations, particularly among fractional covers of trees, cropland, and built-up areas.

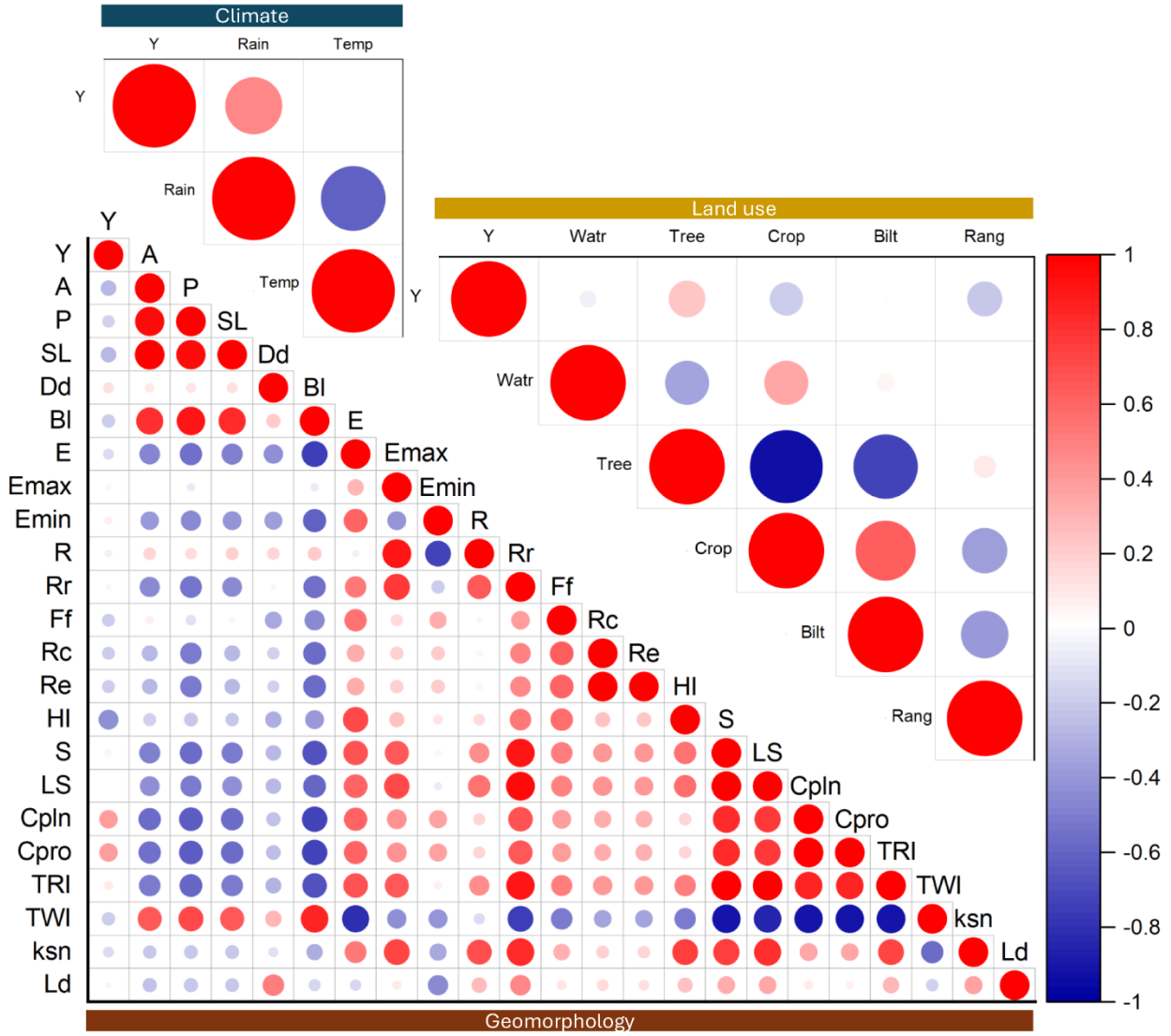

Fig. 6. Correlation matrix of parameters grouped by category: geomorphology, climate, and land use. Bubble size and colour intensity both represent correlation strength (larger/darker = stronger correlation).

The PLSR model summary (Table 3) reveals a complex relationship between explained variance (R^2) and predictive capability (Q^2). While cumulative R^2 for SY increased progressively with component addition (26% for $C_{omp}1$, 39% for $C_{omp}2$, 55% for $C_{omp}3$, 68% for $C_{omp}4$, and 80% for $C_{omp}5$), model quality assessed via cross-validated Q^2 deteriorated markedly. Component 1 yielded a negative Q^2 (-0.22), indicating no predictive improvement over the mean, and subsequent

components showed further degradation ($C_{omp}2$: -0.32; $C_{omp}3$: -1.3; $C_{omp}4$: -1.96; $C_{omp}5$: -3.13). Consequently, only the first component was retained for further analysis.

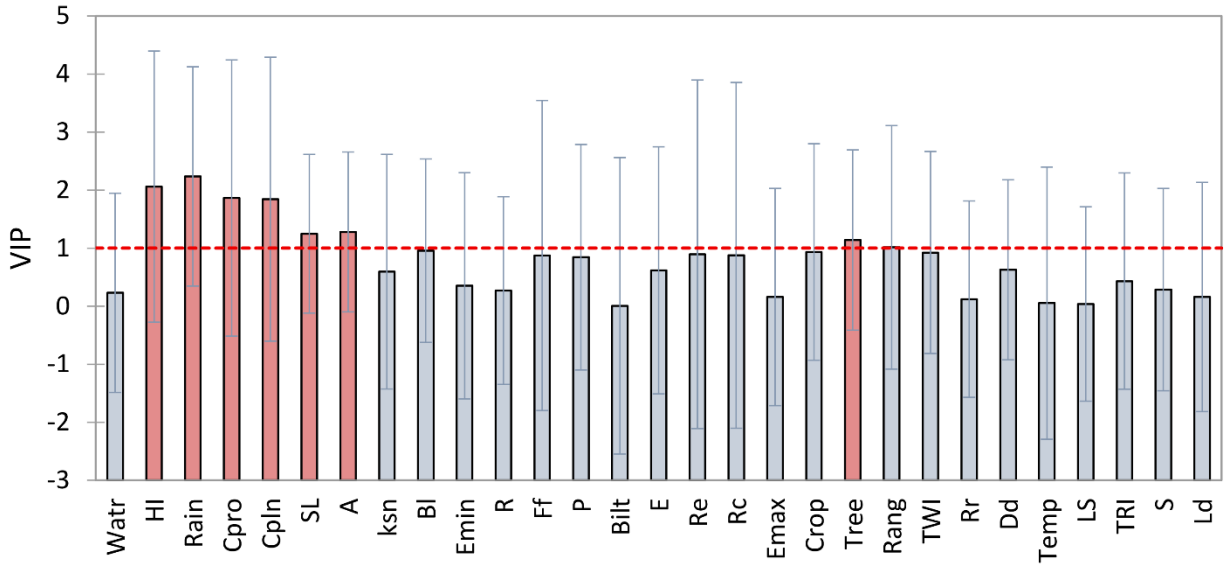

Fig. 7. VIP (Variable Importance in Projection) values per parameter. Values exceeding 1 denote predictors with significant influence.

The VIP calculation identified rainfall (VIP = 2.24), HI (VIP = 2.06), profile curvature (VIP = 1.86), and plan curvature (VIP = 1.84) as the most influential predictors (Fig. 7). Area (VIP = 1.28), stream length (VIP = 1.25), tree cover (VIP = 1.14), and rangeland (VIP = 1.01) also exceeded the significance threshold (VIP > 1). Standardised coefficients (Fig. 8) highlight negative associations between SY and HI, stream length, and area, as well as between SY and tree cover, consistent with its protective role. Conversely, rainfall and cropland exhibited positive coefficient.

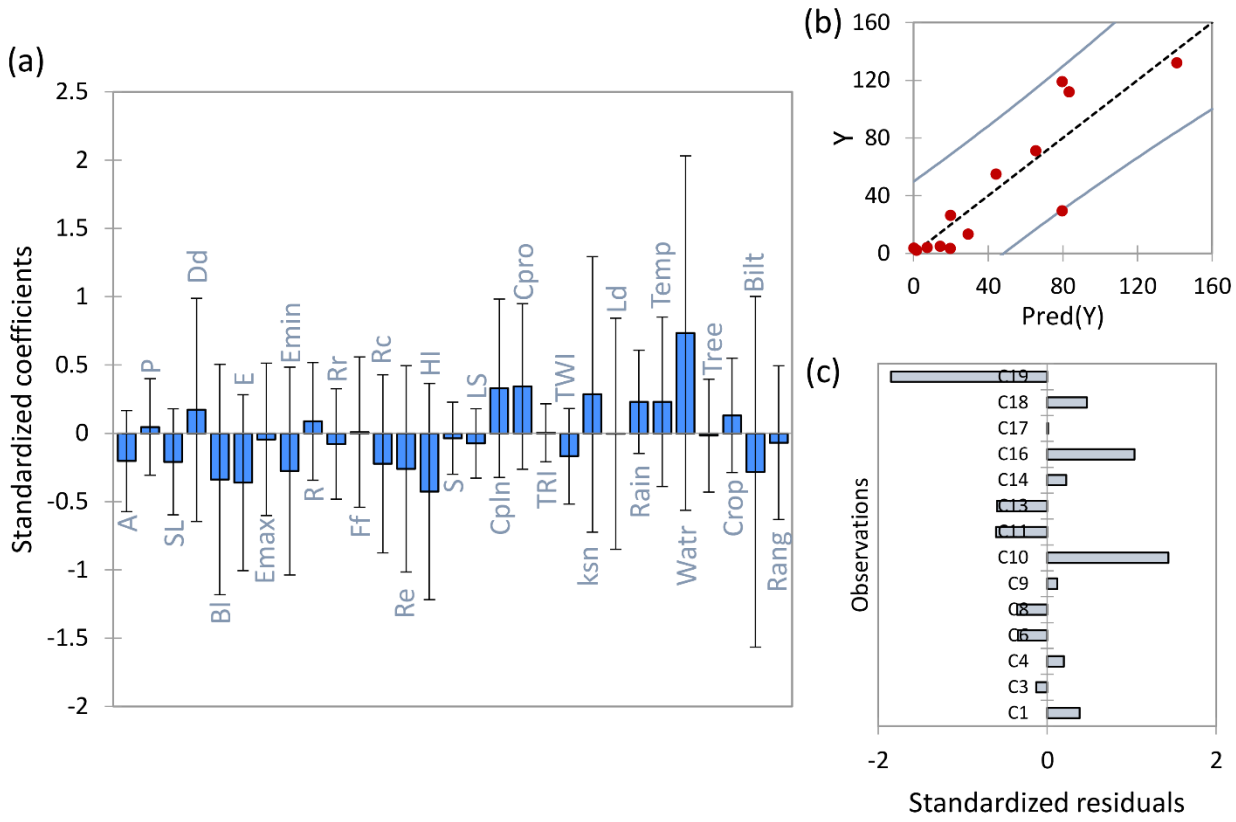

Fig. 8. PLSR model outputs: (a) Standardised coefficients of input parameters; (b) Comparison of predicted and observed outcomes; (c) Spatial distribution of standardised residuals by sub-catchment.

A subsequent PLSR run using only VIP > 1 predictors marginally improved Component 1 Q^2 to 0.13 (R^2 = 29%). However, re-adding components degraded the predictive quality despite higher R^2 values. Thus, while VIP identified the key drivers, PLSR failed to yield a robust predictive SY model.

4.4. Multiple regression in explaining influences:

Complementing PLSR, MLR quantified the explanatory power of predictor categories for SY variance (Fig. 9). Geomorphic parameters collectively explain the highest proportion (53%), surpassing anthropogenic factors (dam capacity + area: 41%), climate variables (35%), and land

use (15%). Notably, the dam area alone captured 41% of the SY variability, closely followed by the dam capacity (36%). Synergistic effects were observed: rainfall combined with elevation explained 37% of variance, while tree/cropland integrated with rainfall explained 29%, and rangeland with rainfall explained 24%. In contrast, fundamental catchment descriptors (area, elevation, and relief) exhibited minimal individual influence (7%, 2%, and 2%, respectively), and temperature demonstrated no significant relationship with SY variation.

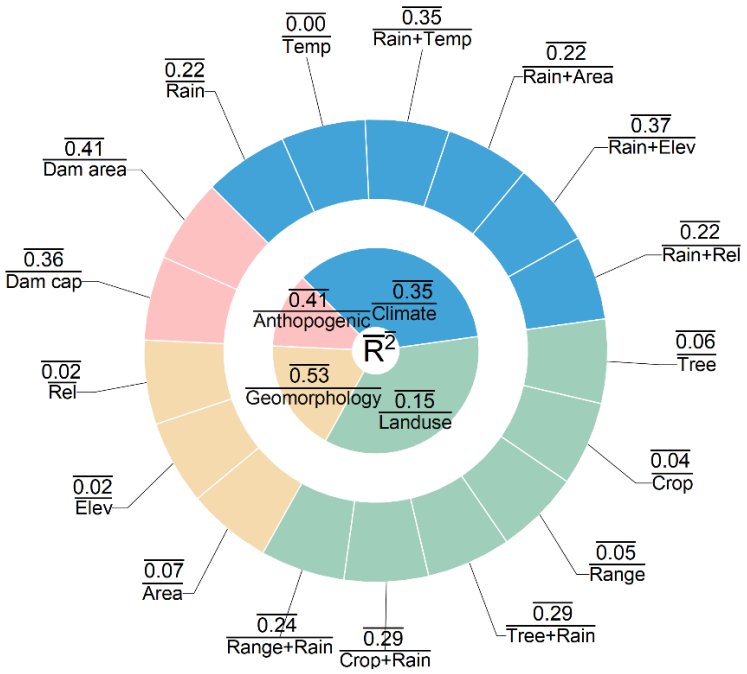

Fig. 9. Comparison of multiple regression models using different combinations of common parameters. The MLR were established considering all the parameters within each group (e.g. geomorphology, climate etc.). Afterwards, different combinations which are generally found common in sediment studies were considered for further investigation.

5. Discussion:

5.1. Geomorphology, topography, and scale dependency as primary controls:

This study reveals that geomorphic parameters are the most influential controls on the variability in sediment yield across the Cauvery Basin. The hypsometric integral, topographic ruggedness index, and plan/profile curvatures emerge as critical indicators of erosional energy and landscape

maturity. A strong negative relationship between sediment yield and hypsometric integral confirms that catchments in a mature erosional stage tend to export more sediment, likely owing to longer slope lengths and well-developed drainage systems, which transport a large volume of sediments (Verstraeten and Poesen 2001). A similar pattern is recorded in the Godavari, the largest catchment of Peninsular India, where sediment yields are higher in basins with lower hypsometric integral (Das et al. 2023). The basin-wide mean hypsometric integral of 0.22 ± 0.10 places the Cauvery firmly within the mature erosional regime, where thick saprolite development on Precambrian granite-gneiss bedrock creates abundant mobile material despite limited uplift (Gunnell and Bourgeon, 1997).

Curvature-based indices show that microtopographic convexity and concavity further modulate local flow concentration and soil detachment potential. Plan curvature controls lateral flow convergence, creating preferential pathways for rill formation on convex ridges (Sofia et al., 2011). Conversely, profile curvature dictates the downslope acceleration of runoff—a critical factor for sediment entrainment on concave slopes. In the Western Ghats sub-catchments (such as C4 and C6), the combination of steep plan and profile curvatures (> 0.01) explains localised spikes in sediment yield. These microtopographic controls interact with the topographic ruggedness index, whose extreme variability potentially reflects the knickpoint availability and migration throughout the Precambrian terrain. This process can maintain a high erosional potential even in mature landscapes (Crosby and Whipple 2006).

Sub-catchment size also emerged as a controlling factor, with sediment yield inversely related to the basin area. This is frequently attributed to increased sediment storage and reduced delivery ratios in larger catchments (Lu et al. 2005; Das et al. 2021). This relationship manifests powerfully across the Cauvery, where the largest sub-catchment (C18: 8,660 km^2) yields merely 5 t km^{-2} yr^{-1}

against 55 t km^{-2} yr^{-1} in the smallest (C1: 592 km^2). This "dilution effect" (de Barros et al. 2021) aligns with findings from other large basins where sediment yield decreases logarithmically with the basin area (e.g., Ayadi et al. 2010; Vanmaercke et al. 2011). This effect is generally a consequence of sediment deposition in low-elevation, low-gradient valleys (Vanmaercke et al. 2014) and sediment trapping at tributary junctions (Fryirs et al. 2007). In the Cauvery, this dilution is amplified by reservoirs intercepting sediment at transitional zones, as evident in mid-sized sub-catchments like C12 (6613 km^2), where negative sediment yield values reflect net deposition >100 kt yr^{-1}. This scale dependency creates disproportionate sediment generation in headwater sub-catchments, while their connectivity to downstream sinks is disrupted by anthropogenic structures.

An important methodological point is the exclusion of geological variability. Lithological variation is known to influence mechanical and chemical weathering (Larimer et al. 2022). For instance, fresh and fine-grained mafic rocks such as basalt exhibit some of the fastest silicate weathering rates (Ibarra et al. 2016; Li et al. 2016), while igneous rocks of felsic properties weather much slowly (West et al. 2005). The Cauvery Basin is largely underlain by homogeneous Precambrian charnockite-granite-gneiss formations, with only minor lithological heterogeneities such as dolerite dykes and metasediments. Given the scale of analysis and almost uniform bedrock properties, geology was not treated as a predictive variable in this study. However, the Cauvery's lithological uniformity provides a natural laboratory where geomorphic signatures emerge clearly.

5.2. Rainfall dominance and temperature disconnection:

The unequivocal dominance of rainfall as the primary climatic control on sediment yield ($R = 0.47$; p-value = 0.09) emphasises the influence of monsoonal hydrology on erosional processes (Fig. 10a). The pronounced orographic gradient resulting in annual rainfall ranging from less than 700 mm yr^{-1} in rain-shadowed central sub-catchments to over 2,500 mm yr^{-1} in windward Western

Ghats sectors creates a stark dichotomy in sediment mobilization. Western sub-catchments (e.g., C4, C6) exhibit sediment yield values up to 132 t km^{-2} yr^{-1}, directly attributable to high-intensity rainfall exceeding soil infiltration capacities. This triggers Hortonian overland flow that simultaneously enhances particle detachment and transport capacity (Zhang et al. 2018). Intense rainfall events (> 50 mm hr^{-1}) are common during summer monsoons and generate peak discharges capable of mobilising coarse sediments that accumulate during drier periods. This rainfall-sediment yield coupling is consistent with what is seen in the Brahmaputra and Godavari, where 70% of the annual sediment flux occurs during peak monsoon (Galy & France-Lanord 2001; Das et al. 2022), confirming the role of precipitation as an erosion agent and sediment conveyor.

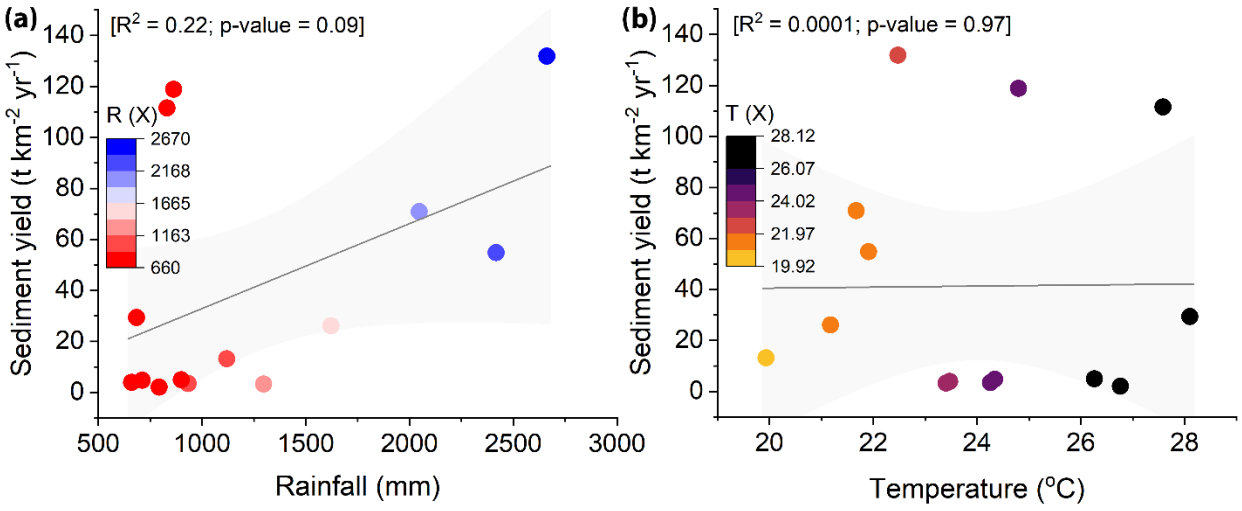

Fig. 10. Association of sediment yield with rainfall and temperature in sub-catchments. Color denotes the concurrent rainfall and temperature values for each data point.

Surprisingly, temperature showed no statistically significant association with the sediment yield (Fig. 10b). The general theoretical expectations are that warmer and wetter conditions accelerate physical weathering via crack-tip molecular bond-breaking (Eppes et al., 2020) and chemical weathering via mineral dissolution (Dixon et al., 2016). Silicate weathering rates (SWR) in tropical

cratons respond logarithmically to temperature and require high differentials for significant effects (West et al., 2005). SWR of the Cauvery basin is higher (13 t km^{-2} $year^{-1}$ at the terminal station Musiri) than several global rivers draining craton/shields (e.g. Congo-Zaire: 4.22 t km^{-2} $year^{-1}$, Tocantins: 7.5 t km^{-2} $year^{-1}$), and is equal to large tropical river like the Amazon (13 t km^{-2} $year^{-1}$) (Upendra et al., 2022). Furthermore, temperature-mediated weathering operates on millennial timescales to produce saprolite, whereas sediment yield chemistry reflects the recent mechanical erosion of Archean gneiss, charnockite and other existing weathered material (Sharma & Rajamani, 2000; Riebe et al., 2004; Sharma & Rajamani, 2001). The formation of a thick saprolith layer on the Precambrian granite restricts chemical weathering (Oliva et al., 2003), is counteracted by the steep slope of the Western Ghats, which provides a suitable setting for the acidic water to chemically react with the saprolith and transform it into saprolite (Rajamani et al., 2009, Nagendra et al., 2020). Hence, in the Cauvery basin, a dynamic equilibrium is maintained between physical (saprolith formation) and chemical weathering (formation of saprolite from saprolith), moderated by rugged topography, presence of structural features, tropical humid climate and dense vegetation (Rajamani et al., 2009). In the Cauvery, thermal mechanisms are less active than the rainfall-induced weathering, despite their theoretical relevance to mineral breakdown.

5.3. Land use and anthropogenic modifications:

Land use patterns significantly influence sediment dynamics, although their effects are more variable and context-dependent than those of topography or rainfall. While global meta-analyses consistently position forests as sediment-suppressing land covers (Fu et al., 2003; Porto et al., 2009), our analysis uncovers a contradictory pattern. Three forest-dominated sub-catchments (> 50% tree cover) rank among the highest sediment yield producers, while three others with comparable forest cover exhibit the lowest yields. Linear regression analyses highlight a negative

494 association where low sediment yield sub-catchments comprise higher agricultural land than
495 forested areas and vice versa (Fig. 11). This apparent contradiction reduces from the spatial
496 coupling of land use with geomorphic and climatic drivers.

497 Forested areas predominantly occupy the high-relief, high-rainfall (> 2000 mm yr^{-1}) Western
498 Ghats, where extreme orographic rainfall frequently exceeds the infiltration capacity and triggers
499 saturated overland flow (Putty & Prasad, 2000) and mass wasting (Islam et al., 2025). Conversely,
500 croplands dominate the low-elevation eastern plains (rainfall < 800 mm yr^{-1}), where limited runoff
501 energy constrains sediment mobilisation despite the high erosive potential from surface exposure.
502 This spatial decoupling creates statistical artefacts where the PLSR coefficients associate forests
503 with negative sediment yield and croplands with positive sediment yield, masking the reality that
504 when forests coincide with extreme topography and rainfall, they fail to prevent erosion. On the
505 other hand, croplands in low-energy environments exhibit limited sediment export (Das et al.,
506 2023).

507 In general, this mechanism follows a U-shaped relationship between tree cover and sediment yield,
508 while an intermediate cover optimises erosion control through root reinforcement and canopy
509 interception, but high-density forests in extreme environments accelerate sediment production
510 through enhanced biogenic weathering and concentrated flow paths along decaying root channels
511 (Ghestem et al., 2011). In the Western Ghats, these processes can lead to the transport of weathered
512 regolith from beneath forest canopies. The Godavari Basin exhibits identical patterns where
513 forested headwaters contribute large sediment amounts and demonstrate land use functions within
514 a process hierarchy dominated by the physiographic context (Das et al., 2023).

515

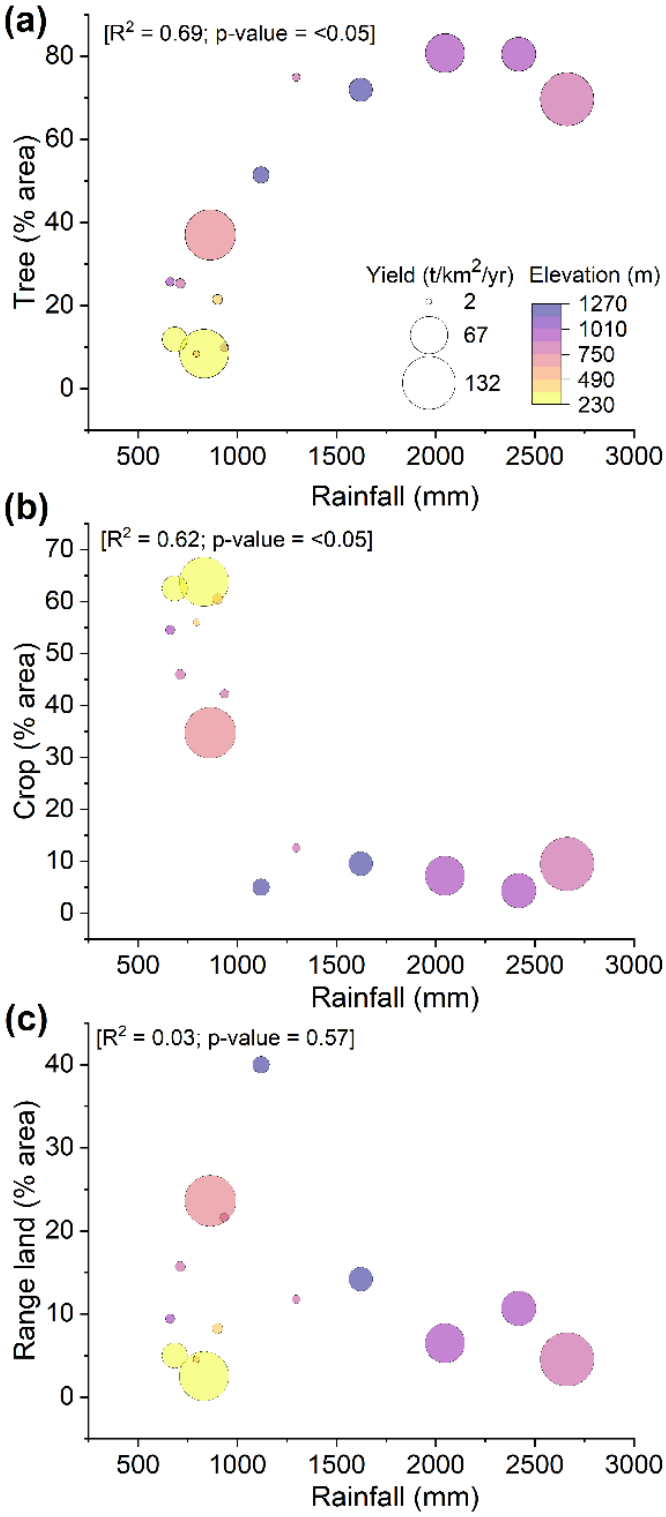

516

517 Fig. 11. Association of rainfall with (a) tree coverage, (b) crop area, and (c) rangeland. Sediment
518 yield is represented by bubble size, and elevation is denoted by colour variation.

519

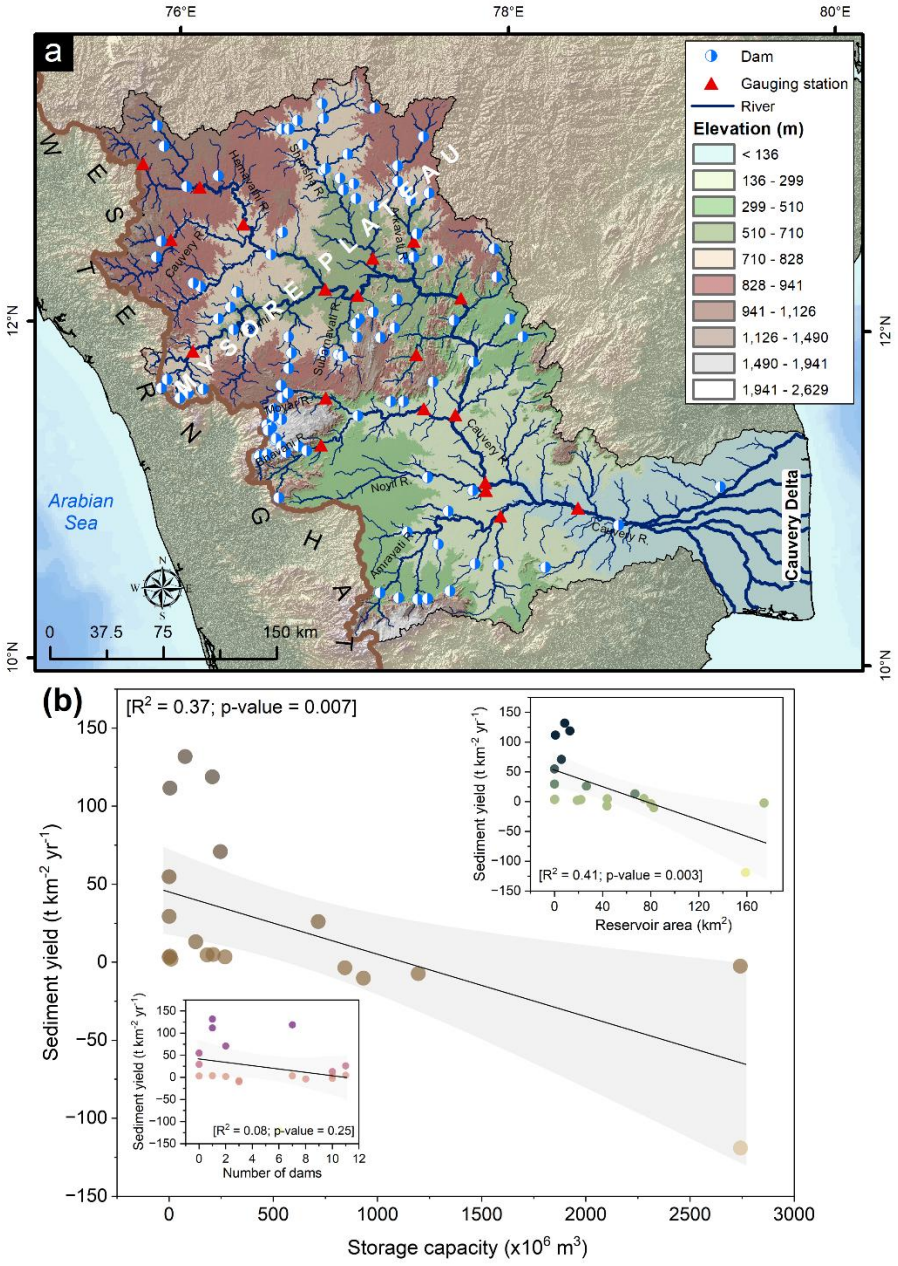

520

521 Fig. 12. (a) Distribution of large dams within the Cauvery basin. (b) Association between storage
522 capacity and sediment yield for the sub-catchments considered in this study. Insets show the
523 association of reservoir area and number of dams with sediment yield.

524

525 The detection of negative sediment yields in five reservoir-associated sub-catchments (C2, C5, C7,

526 C12, C15) represents a definitive anthropogenic signature within the basin's sediment cascade.

These values signify profound sediment retention where upstream sediment influx exceeds downstream outflow, which reflects near-total trapping within impoundments. Currently, 96 large multipurpose dams (CWC, 2019b) exist in the basin that alter the longitudinal sediment connectivity of the channel. Quantitatively, dam infrastructure alone explains 41% of the sediment yield variation through dam area and 37% through storage capacity (p-value = < 0.05), surpassing both land use (15%) and climatic drivers (35%) in predictive power (Fig. 12). This dominance demonstrates how engineering interventions override the basin's natural sediment dynamics and corroborates global patterns where dams reduce downstream sediment flux. These impoundments disproportionately affect transitional mid-basin sub-catchments (e.g., C5: 7833 km^2) and intercepting sediments from high-yield headwaters before they reach the terminal gauges.

This 'hungry water' (Kondolf, 1997) released from the dams with a very low amount of sediment regains its energy to erode the channel and incur changes in downstream channel morphology. The disproportionate rapid increase of sediment yield in a floodplain mid-size sub-catchment (C16) can probably be explained by this effect, where sediment-starved, highly erosive water from Mettur dam and Lower Bhavani dam confluences and causes significant erosion. Consequently, while geomorphic parameters govern potential sediment production, reservoirs control its actual delivery and effectively decouple hillslope erosion from basin-scale sediment discharge. This hierarchy demonstrates a fundamental Anthropocene alteration where human infrastructure now mediates sediment regimes more powerfully than bedrock geology or precipitation gradients in regulated basins globally (Das et al., 2025; Syvitski et al., 2005; Vörösmarty et al., 2003).

6. Conclusion:

This study explained the hierarchical controls governing the spatial heterogeneity of sediment yields in the anthropogenically modified Cauvery Basin, India. Geomorphic parameters,

principally hypsometric integral and topographic curvatures (plan and profile), emerged as the dominant intrinsic factors. The basin-wide low mean hypsometric integral (0.22 ± 0.10) signifies a mature erosional landscape where extensive weathered regolith on Precambrian basement is accumulated, and the localised steep plan and profile curvature (> 0.01) facilitates sediment mobilisation despite the limited tectonic forcing.

The strong inverse relationship between sediment yield and basin area denotes a fundamental scale dependency, where larger catchments exhibit significantly reduced specific yields due to enhanced sediment storage and trapping by floodplains and anthropogenic structures. Rainfall explicitly dominates climatic controls, with its pronounced orographic gradient directly driving SY patterns through intense monsoonal events. Conversely, the limited thermal variability across the basin made temperature statistically insignificant for sediment yield, which highlights the disconnection between long-term weathering processes and shorter-term mechanical sediment export in this tropical monsoonal setting.

While significant, land use impacts are proven to be highly context-dependent and spatially coupled with geomorphic and climatic drivers. High forest cover coinciding with highly elevated, steep, high-rainfall terrain failed to suppress erosion, while cropland expansion in lower-energy environments showed limited sediment export.

Furthermore, dam infrastructure emerged as an important anthropogenic control, overriding natural drivers by intercepting sediment fluxes. Dam area and storage capacity alone explained 41% and 36% of sediment yield variability, demonstrating a profound decoupling between the hillslope erosion potential and basin-scale sediment delivery.

These findings have important implications for sustainable water and sediment management in the Cauvery Basin. Quantifying the dominance of geomorphic maturity and rainfall intensity enables targeted prioritisation of erosion control measures in high-yield headwater sub-catchments. The impact of dams necessitates integrating sediment continuity assessments into reservoir operations planning to mitigate downstream starvation. Furthermore, the identified control hierarchy provides a robust conceptual framework for improving predictive sediment yield models in anthropogenically altered landscapes, which is essential for adapting water resource infrastructure to climate intensification.

Authors contribution:

Sumit Das: Conceptualization, Methodology, Visualization, Validation, Supervision, Writing- original draft. **Soumi Talukdar:** Methodology, Visualization, Formal analysis, Writing- original draft. **Gianvito Scaringi:** funding, Validation, Writing- review and editing.

Acknowledgements

The authors acknowledge financial support from the Ministry of Education, Culture and Sport of the Czech Republic (MSMT ERC CZ grant No. LL2316) and the Czech Science Foundation (grant No. 24-12316S).

References:

Abdi, H. (2009). Partial least squares regression and projection on latent structure regression (PLS Regression). Wiley Interdisciplinary Reviews: Computational Statistics, 2(1), 97-106. https://doi.org/10.1002/wics.51

Ayadi, I., Abida, H., Djebbar, Y., & Raouf Mahjoub, M. (2010). Sediment yield variability in central Tunisia: a quantitative analysis of its controlling factors. *Hydrological Sciences Journal*, 55(3), 446–458. https://doi.org/10.1080/02626661003741526

Berry, P., Garlick, J., & Smith, R. (2006). Near-global validation of the SRTM DEM using satellite radar altimetry. *Remote Sensing of Environment*, *106*(1), 17–27. https://doi.org/10.1016/j.rse.2006.07.011

Bhattacharjee, S., Bookhagen, B., & Sinha, R. (2022). Sediment-transport rates from decadal to millennial timescales across the Indo-Gangetic Plain: Impacts of tectonics, climatic processes, and vegetation cover. *Earth-Science Reviews*, 233, 104165. https://doi.org/10.1016/j.earscirev.2022.104165

Bookhagen, B., Thiede, R. C., & Strecker, M. R. (2005). Abnormal monsoon years and their control on erosion and sediment flux in the high, arid northwest Himalaya. *Earth and Planetary Science Letters*, 231(1-2), 131-146. https://doi.org/10.1016/j.epsl.2004.11.014

Chaubey, P. K., & Mall, R. K. (2023). Intensification of Extreme Rainfall in Indian River Basin: Using Bias Corrected CMIP6 Climate Data. *Earth's Future*, 11(9), e2023EF003556. https://doi.org/10.1029/2023EF003556

Chidambaram, S.; Ramanathan, A.; Thilagavathi, R.; & Ganesh, N. (2019). Physiography, Cauvery River. In Indian rivers: Scientific and socio-economic aspects. (p. 354). Springer.

Crosby, B. T., & Whipple, K. X. (2006). Knickpoint initiation and distribution within fluvial networks: 236 waterfalls in the Waipaoa River, North Island, New Zealand. *Geomorphology*, 82(1-2), 16-38. https://doi.org/10.1016/j.geomorph.2005.08.023

CWC (2014) Cauvery Basin v. 2.0. Ministry of Water Resources, Govt. of India.
CWC (2019a) Water Year Book Cauvery Basin. Central Water Commission. Govt. of India.
CWC (2019b) National register of large dams – 2019. Central Water Commission, Govt. of India.

Das, S. (2021). Dynamics of streamflow and sediment load in Peninsular Indian rivers (1965–2015). *Science of The Total Environment*, 799, 149372. https://doi.org/10.1016/j.scitotenv.2021.149372

Das, S., Jadhav, H., Roy, A., Scaringi, G., 2025. Sediment load decline and increased erosion linked to human activities in the Cauvery delta, India. Catena (under review).

Das, S., Sangode, S. J., & Kandekar, A. M. (2021). Recent decline in streamflow and sediment discharge in the Godavari basin, India (1965–2015). *CATENA*, 206, 105537. https://doi.org/10.1016/j.catena.2021.105537

Das, S., Sangode, S. J., Kandekar, A. M., Meshram, D. C., & Tarolli, P. (2023). Interrelation between factors controlling sediment yield in the largest catchment of Peninsular India. *Journal of Hydrology*, 622, 129680. https://doi.org/10.1016/j.jhydrol.2023.129680

Das, S., Kandekar, A. M., & Sangode, S. J. (2022). Natural and anthropogenic effects on spatio-temporal variation in sediment load and yield in the Godavari basin, India. *Science of The Total Environment*, 845, 157213. https://doi.org/10.1016/j.scitotenv.2022.157213

Das, S., Yunus, A. P., Scaringi, G., & Narayana, A. (2025). Local and broad-scale anthropogenic controls on sediment transport in the Western Ghats rivers, India. *Anthropocene*, 100485. https://doi.org/10.1016/j.ancene.2025.100485

De Barros, C. A. P., Govers, G., Minella, J. P. G., & Ramon, R. (2021). How water flow components affect sediment dynamics modeling in a Brazilian catchment. *Journal of Hydrology*, 597, 126111. https://doi.org/10.1016/j.jhydrol.2021.126111

Poesen, J., Bazzoffi, P., Rompaey, A. V., & Verstraeten, G. (2006). Predicting catchment sediment yield in Mediterranean environments: The importance of sediment sources and connectivity in Italian drainage basins. Earth Surface Processes and Landforms, 31(8), 1017-1034. https://doi.org/10.1002/esp.1305

De Vente, J., Poesen, J., Verstraeten, G., Govers, G., Vanmaercke, M., Van Rompaey, A., Arabkhedri, M., & Boix-Fayos, C. (2013). Predicting soil erosion and sediment yield at regional scales: Where do we stand? *Earth-Science Reviews*, 127, 16-29. https://doi.org/10.1016/j.earscirev.2013.08.014

Dixon, J. L., Chadwick, O. A., & Vitousek, P. M. (2016). Climate-driven thresholds for chemical weathering in postglacial soils of New Zealand. *Journal of Geophysical Research: Earth Surface*, 121(9), 1619-1634. https://doi.org/10.1002/2016JF003864

Donovan, M., & Monaghan, R. (2021). Impacts of grazing on ground cover, soil physical properties and soil loss via surface erosion: A novel geospatial modelling approach. *Journal of Environmental Management*, 287, 112206. https://doi.org/10.1016/j.jenvman.2021.112206

Ekka, A., Keshav, S., Pande, S., Van der Zaag, P., & Jiang, Y. (2022). Dam-induced hydrological alterations in the upper Cauvery river basin, India. *Journal of Hydrology: Regional Studies*, 44, 101231. https://doi.org/10.1016/j.ejrh.2022.101231

Eppes, M. C., Magi, B., Scheff, J., Warren, K., Ching, S., & Feng, T. (2020). Warmer, wetter climates accelerate mechanical weathering in field data, independent of Stress-Loading. *Geophysical Research Letters*, *47*(24). https://doi.org/10.1029/2020gl089062

Fryirs, K. A., Brierley, G. J., Preston, N. J., & Kasai, M. (2007). Buffers, barriers and blankets: The (dis)connectivity of catchment-scale sediment cascades. *CATENA*, 70(1), 49-67. https://doi.org/10.1016/j.catena.2006.07.007

Fu, B., Wang, J., Chen, L., & Qiu, Y. (2003). The effects of land use on soil moisture variation in the Danangou catchment of the Loess Plateau, China. *CATENA*, 54(1-2), 197-213. https://doi.org/10.1016/S0341-8162(03)00065-1

Galy, A., France-Lanord, C., 2001. Higher erosion rates in the Himalaya: Geochemical constraints on riverine fluxes. *Geology*, 29(1), 23-26. https://doi.org/10.1130/0091-7613(2001)029<0023:HERITH>2.0.CO;2

Ghestem, M., Sidle, R. C., & Stokes, A. (2011). The Influence of Plant Root Systems on Subsurface Flow: Implications for Slope Stability. *BioScience*, 61(11), 869-879. https://doi.org/10.1525/bio.2011.61.11.6

Gosain, A. K., Rao, S., & Basuray, D. (2006). Climate change impact assessment on hydrology of Indian river basins. *Current Science*, 90(3), 346-353.

Gowri, R., Dey, P., & Mujumdar, P. (2021). A hydro-climatological outlook on the long-term availability of water resources in Cauvery river basin. *Water Security*, 14, 100102. https://doi.org/10.1016/j.wasec.2021.100102

Gupta, H., Kao, S., & Dai, M. (2012). The role of mega dams in reducing sediment fluxes: A case study of large Asian rivers. *Journal of Hydrology*, 464-465, 447-458. https://doi.org/10.1016/j.jhydrol.2012.07.038

Gunnell, Y., & Bourgeon, G. (1997). Soils and climatic geomorphology on the Karnataka plateau, peninsular India. *CATENA*, 29(3-4), 239-262. https://doi.org/10.1016/S0341-8162(96)00070-7

Hariprasad, K.M., Pushpalatha, R., Singh, B., Roshni, T., 2024. Linking future soil erosion and sediment yield in the upper Cauvery sub-basin: a modeling framework using CMIP6 data. 15th Int. Conf. Comp. Comm. Net. Tech. Doi: 10.1109/ICCCNT61001.2024.10724237.

Haritashya, U. K., Singh, P., Kumar, N., & Gupta, R. (2005). Suspended sediment from the Gangotri Glacier: Quantification, variability and associations with discharge and air temperature. *Journal of Hydrology*, *321*(1–4), 116–130. https://doi.org/10.1016/j.jhydrol.2005.07.037

Hijmans, R. J., Cameron, S. E., Parra, J. L., Jones, P. G., & Jarvis, A. (2005). Very high resolution interpolated climate surfaces for global land areas. *International Journal of Climatology*, *25*(15), 1965–1978. https://doi.org/10.1002/joc.1276

Hirschberg, J., Fatichi, S., Bennett, G. L., McArdell, B. W., Peleg, N., Lane, S. N., Schlunegger, F., & Molnar, P. (2020). Climate Change Impacts on Sediment Yield and Debris-Flow Activity in an Alpine Catchment. *Journal of Geophysical Research: Earth Surface*, 126(1), e2020JF005739. https://doi.org/10.1029/2020JF005739

Ibarra, D. E., Caves, J. K., Moon, S., Thomas, D. L., Hartmann, J., Chamberlain, C. P., & Maher, K. (2016). Differential weathering of basaltic and granitic catchments from concentration–discharge relationships. *Geochimica et Cosmochimica Acta*, 190, 265-293. https://doi.org/10.1016/j.gca.2016.07.006

Islam, S., Thanveer, J., Yunus, A. P., Beetan, Y., Umrikar, B., Arya, D. S., & Subramanian, S. S. (2025). Impact of antecedent rainfall and soil saturation on widespread debris flows in the northern Western Ghats during the 2021 extreme rainfall. *Bulletin of Engineering Geology and the Environment*, *84*(7). https://doi.org/10.1007/s10064-025-04383-z

Jadhav, H., Kandekar, A. M., & Das, S. (2023). Climatic and Anthropogenic Influences on Long-Term Discharge and Sediment Load Changes in the Second-Largest Peninsular Indian Catchment. *Water*, 16(24), 3648. https://doi.org/10.3390/w16243648

Kale, V. S., Sengupta, S., Achyuthan, H., & Jaiswal, M. K. (2014). Tectonic controls upon Kaveri River drainage, cratonic Peninsular India: Inferences from longitudinal profiles, morphotectonic indices, hanging valleys and fluvial records. *Geomorphology*, 227, 153-165. https://doi.org/10.1016/j.geomorph.2013.07.027

Kondolf, G. M. (1997), Hungry water: Effects of dams and gravel mining on river channels, *Environmental Management*, 21(4), 533–551.

Larimer, J. E., Yanites, B. J., & Jung, S. J. (2022). A Field Study on the Lithological Influence on the Interaction Between Weathering and Abrasion Processes in Bedrock Rivers. *Journal of Geophysical Research: Earth Surface*, 127(4), e2021JF006418. https://doi.org/10.1029/2021JF006418

Li, D., Zhang, T., Walling, D. E., Lane, S., Bookhagen, B., Tian, S., Overeem, I., Syvitski, J., Kettner, A. J., Park, E., Koppes, M., P. Schmitt, R. J., Sun, W., Ni, J., & Ehlers, T. A. (2024). The competing controls of glaciers, precipitation, and vegetation on high-mountain fluvial sediment yields. *Science Advances*. https://doi.org/ads6196

Li, G., Hartmann, J., Derry, L. A., West, A. J., You, C., Long, X., Zhan, T., Li, L., Li, G., Qiu, W., Li, T., Liu, L., Chen, Y., Ji, J., Zhao, L., & Chen, J. (2016). Temperature dependence of basalt weathering. *Earth and Planetary Science Letters*, 443, 59-69. https://doi.org/10.1016/j.epsl.2016.03.015

Li, Z., Xu, X., Zhu, J., Xu, C., & Wang, K. (2019). Effects of lithology and geomorphology on sediment yield in karst mountainous catchments. *Geomorphology*, 343, 119–128. https://doi.org/10.1016/j.geomorph.2019.07.001

Li, D., Overeem, I., Kettner, A. J., Zhou, Y., & Lu, X. (2021). Air temperature regulates erodible landscape, water, and sediment fluxes in the Permafrost-Dominated catchment on the Tibetan Plateau. *Water Resources Research*, *57*(2). https://doi.org/10.1029/2020wr028193

Lu, H., Moran, C. J., & Sivapalan, M. (2005). A theoretical exploration of catchment-scale sediment delivery. *Water Resources Research*, 41(9). https://doi.org/10.1029/2005WR004018

Lu, X., & Higgitt, D. L. (1999). Sediment yield variability in the Upper Yangtze, China. *Earth Surface Processes and Landforms*, 24(12), 1077-1093. https://doi.org/10.1002/(SICI)1096-9837(199911)24:12<1077::AID-ESP36>3.0.CO;2-M

Majhi, A., Shaw, R., Mallick, K., & Patel, P. P. (2021). Towards improved USLE-based soil erosion modelling in India: A review of prevalent pitfalls and implementation of exemplar methods. *Earth-Science Reviews*, 221, 103786. https://doi.org/10.1016/j.earscirev.2021.103786

Milliman, J.D., Farnsworth, K.L., 2011. River Discharge to the Coastal Ocean: A Global Synthesis. Cambridge University Press, Cambridge.

Nadal-Romero, E., Vicente-Serrano, S., Lana-Renault, N., López-Moreno, J. I., Regües, D., Lasanta, T., & García-Ruiz, J. M. (2025). Plant cover determines runoff generation in response to dry and wet conditions. *Journal of Hydrology*, 660, 133495. https://doi.org/10.1016/j.jhydrol.2025.133495

Nagendra, R., Elango, L., & Vybhav, K. (2020). Spatial and Temporal Variations in the Geochemistry of Cauvery River (Tamil Nadu, India) Sediments and its Implication to Weathering. *Indian Association of Sedimentologists*, *37*(2), 49–60. https://doi.org/10.51710/jias.v37i2.107

Narasimha Chari, M., Sahu, J., Banerjee, B., Zutshi, P., & Chandra, K. (1994). Evolution of the Cauvery basin, India from subsidence modelling. *Marine and Petroleum Geology*, 12(6), 667-675. https://doi.org/10.1016/0264-8172(95)98091-I

Olen, S. M., Bookhagen, B., & Strecker, M. R. (2016). Role of climate and vegetation density in modulating denudation rates in the Himalaya. Earth and Planetary Science Letters, 445, 57-67. https://doi.org/10.1016/j.epsl.2016.03.047

Oliva, P., Viers, J., & Dupré, B. (2003). Chemical weathering in granitic environments. *Chemical Geology*, *202*(3–4), 225–256. https://doi.org/10.1016/j.chemgeo.2002.08.001

Panagos, P., Ballabio, C., Meusburger, K., Spinoni, J., Alewell, C., & Borrelli, P. (2017). Towards estimates of future rainfall erosivity in Europe based on REDES and WorldClim datasets. *Journal of Hydrology*, *548*, 251–262. https://doi.org/10.1016/j.jhydrol.2017.03.006

Poesen, J., Bazzoffi, P., Rompaey, A. V., & Verstraeten, G. (2006). Predicting catchment sediment yield in Mediterranean environments: The importance of sediment sources and connectivity in Italian drainage basins. *Earth Surface Processes and Landforms*, 31(8), 1017-1034. https://doi.org/10.1002/esp.1305

Porto, P., Walling, D. E., & Callegari, G. (2009). Investigating the effects of afforestation on soil erosion and sediment mobilisation in two small catchments in Southern Italy. *CATENA*, 79(3), 181-188. https://doi.org/10.1016/j.catena.2009.01.007

Poyil, R.P., Dhanalakshmi, S., Goyal, P., 2016. Predicting future changes in climate and its impact on changes in land use: a case study of Cauvery basin. *Proc. SPIE 9877, Land Surf. Cryos. Remote Sens. III*, 98772Y. https://doi.org/10.1117/12.2223531

Putty, M., & Prasad, R. (2000). Understanding runoff processes using a watershed model—a case study in the Western Ghats in South India. *Journal of Hydrology*, *228*(3–4), 215–227. https://doi.org/10.1016/s0022-1694(00)00141-4

Rajamani, V., Tripathi, J. K., & Malviya, V. (2009). Weathering of lower crustal rocks in the Kaveri river catchment, southern India: Implications to sediment geochemistry. *Chemical Geology*, *265*(3–4), 410–419. https://doi.org/10.1016/j.chemgeo.2009.05.007

Ramanathan, A.L., Subramanian, V. & Das, B.K. (1996) Sediment and heavy metal accumulation in the Cauvery basin. *Environmental Geology*, 27, 155–163. https://doi.org/10.1007/BF00770427

Rehana, S., & Mujumdar, P. (2012). Climate change induced risk in water quality control problems. *Journal of Hydrology*, *444–445*, 63–77. https://doi.org/10.1016/j.jhydrol.2012.03.042

Restrepo, J. D., Kjerfve, B., Hermelin, M., & Restrepo, J. C. (2006). Factors controlling sediment yield in a major South American drainage basin: The Magdalena River, Colombia. *Journal of Hydrology*, 316(1-4), 213-232. https://doi.org/10.1016/j.jhydrol.2005.05.002

Riebe, C. S., Kirchner, J. W., & Finkel, R. C. (2004). Erosional and climatic effects on long-term chemical weathering rates in granitic landscapes spanning diverse climate regimes. *Earth and Planetary Science Letters*, 224(3-4), 547-562. https://doi.org/10.1016/j.epsl.2004.05.019

Samal, P., Swain, P. C., & Samantaray, S. (2024). GIS-based RUSLE model for estimating soil erosion and sediment yield in Rushikulya River Basin of Odisha, India. *Journal of Earth System Science,* 133(4). https://doi.org/10.1007/s12040-024-02458-1

Sajeev, K. (2021). The tectonic and metamorphic perspective of Southern Granulite Terrane, India. *Journal of the Geological Society of India*, 97(9), 1112–1112. https://doi.org/10.1007/s12594-021-1830-z

Sharma, A., & Rajamani, V. (2001). Weathering of charnockites and sediment production in the catchment area of the Cauvery River, southern India. *Sedimentary Geology*, *143*(1–2), 169–184. https://doi.org/10.1016/s0037-0738(01)00102-6

Sharma, A., & Rajamani, V. (2000). Weathering of gneissic rocks in the upper reaches of Cauvery river, south India: implications to neotectonics of the region. *Chemical Geology*, *166*(3–4), 203–223. https://doi.org/10.1016/s0009-2541(99)00222-3

Shi, Z., Huang, X., Ai, L., Fang, N., & Wu, G. (2014). Quantitative analysis of factors controlling sediment yield in mountainous watersheds. *Geomorphology*, 226, 193-201. https://doi.org/10.1016/j.geomorph.2014.08.012

Shcheglova, O. P., & Chizhov, O. P. (1981). Sediment Transport from the Glacier Zone, Central Asia. *Annals of Glaciology*, *2*, 103–108. https://doi.org/10.3189/172756481794352324

Shukla, A. K., Ojha, C. S. P., Mijic, A., Buytaert, W., Pathak, S., Garg, R. D., & Shukla, S. (2018). Population growth, land use and land cover transformations, and water quality nexus in the Upper Ganga River basin. *Hydrology and Earth System Sciences*, *22*(9), 4745–4770. https://doi.org/10.5194/hess-22-4745-2018

Singh, P., Haritashya, U. K., Ramasastri, K. S., & Kumar, N. (2004). Diurnal variations in discharge and suspended sediment concentration, including runoff-delaying characteristics, of the Gangotri Glacier in the Garhwal Himalayas. *Hydrological Processes*, *19*(7), 1445–1457. https://doi.org/10.1002/hyp.5583

Singh, J., Singh, M. C., & Mathur, A. (2025). Assessment of reservoir capacity and sedimentation rate in Chohal Dam, Punjab, India, using multi-satellite data. *Water Science & Technology Water Supply*. https://doi.org/10.2166/ws.2025.055

Sofia,G., Tarolli, P., Cazorzi, F., Fontana, D., 2011. An objective approach for feature extraction: distribution analysis and statistical descriptors for scale choice and channel network identification. *Hydrology and Earth System Sciences*, 15, 1387-1402. https://doi.org/10.5194/hess-15-1387-2011

Syvitski, J., Ángel, J. R., Saito, Y., Overeem, I., Vörösmarty, C. J., Wang, H., & Olago, D. (2022). Earth's sediment cycle during the Anthropocene. *Nature Reviews Earth & Environment*, 3(3), 179-196. https://doi.org/10.1038/s43017-021-00253-w

Syvitski, J. P. M., Kettner, A. J., & Green, P. (2005). Impact of Humans on the Flux of Terrestrial Sediment to the Global Coastal Ocean. *Science*, 308(5720), 376-380. https://doi.org/10.1126/science.1109454

Tan, Y., Liu, H., & Lu, Y. (2023). Sediment yield in the Lower Jinsha River Basin, China: Controlling factors and spatiotemporal patterns. *CATENA*, 229, 107236. https://doi.org/10.1016/j.catena.2023.107236

Twinkle, D.; Rao, G. S.; Radhakrishna, M.; & Murthy, K. S. (2016). Crustal structure and rift tectonics across the cauvery–palar basin, eastern continental margin of India based on seismic and potential field modelling. *Journal of Earth System Science*, 125(2), 329–342. https://doi.org/10.1007/s12040-016-0669-y

Upendra, B., Ciba, M., Aiswarya, A., Dev, V. V., Sreenivasulu, G., & Krishnan, K. A. (2022). Mechanisms controlling the dissolved load, chemical weathering and CO2 consumption rates of Cauvery River, South India: role of secondary soil minerals. *Environmental Earth Sciences*, *81*(3). https://doi.org/10.1007/s12665-022-10222-1

Vaithiyanathan, P., Ramanathan, A., & Subramanian, V. (1992). Sediment transport in the Cauvery River basin: Sediment characteristics and controlling factors. Journal of Hydrology, 139(1-4), 197-210. https://doi.org/10.1016/0022-1694(92)90202-7

Vanmaercke, M., Poesen, J., Broeckx, J., & Nyssen, J. (2014). Sediment yield in Africa. *Earth-Science Reviews*, 136, 350-368. https://doi.org/10.1016/j.earscirev.2014.06.004

Vanmaercke, M., Poesen, J., Govers, G., & Verstraeten, G. (2015). Quantifying human impacts on catchment sediment yield: A continental approach. Global and Planetary Change, 130, 22-36. https://doi.org/10.1016/j.gloplacha.2015.04.001

Vanmaercke, M., Poesen, J., Verstraeten, G., De Vente, J., & Ocakoglu, F. (2011). Sediment yield in Europe: Spatial patterns and scale dependency. *Geomorphology*, 130(3-4), 142-161. https://doi.org/10.1016/j.geomorph.2011.03.010

Verstraeten, G., & Poesen, J. (2001). Factors controlling sediment yield from small intensively cultivated catchments in a temperate humid climate. *Geomorphology*, 40(1-2), 123-144. https://doi.org/10.1016/S0169-555X(01)00040-X

Vörösmarty, C. J., Meybeck, M., Fekete, B., Sharma, K., Green, P., & Syvitski, J. P. (2003). Anthropogenic sediment retention: Major global impact from registered river impoundments. *Global and Planetary Change*, 39(1-2), 169-190. https://doi.org/10.1016/S0921-8181(03)00023-7

Walling, D., & Fang, D. (2003). Recent trends in the suspended sediment loads of the world's rivers. *Global and Planetary Change*, 39(1-2), 111-126. https://doi.org/10.1016/S0921-8181(03)00020-1

West, A. J., Galy, A., & Bickle, M. (2005). Tectonic and climatic controls on silicate weathering. *Earth and Planetary Science Letters*, 235(1-2), 211-228. https://doi.org/10.1016/j.epsl.2005.03.020

Wold, S., Sjöström, M., & Eriksson, L. (2001). PLS-regression: A basic tool of chemometrics. *Chemometrics and Intelligent Laboratory Systems*, 58(2), 109-130. https://doi.org/10.1016/S0169-7439(01)00155-1

Yan, B., Fang, N., Zhang, P., & Shi, Z. (2013). Impacts of land use change on watershed streamflow and sediment yield: An assessment using hydrologic modelling and partial least squares regression. *Journal of Hydrology*, 484, 26-37. https://doi.org/10.1016/j.jhydrol.2013.01.008

Yunus, A.P., Ishan, A., Magesh, N.S., Sajinkumar, K.S., Scaringi, G., Subramanian, S.S., Oommen, T., 2025. Rapid evacuation of suspended sediment loads during landslides in steep gradient rivers. Env. Res. Comm. 7, 031002.

Zhang, X., & Cai, X. (2011). Climate change impacts on global agricultural land availability. *Environmental Research Letters*, 6(1), 014014. https://doi.org/10.1088/1748-9326/6/1/014014

Zhang, H., Shi, Z., Fang, N., & Guo, M. (2015). Linking watershed geomorphic characteristics to sediment yield: Evidence from the Loess Plateau of China. *Geomorphology*, 234, 19-27. https://doi.org/10.1016/j.geomorph.2015.01.014

Zhang, Q., Wang, Z., Wu, B., Shen, N., & Liu, J. (2018). Identifying sediment transport capacity of raindrop-impacted overland flow within transport-limited system of interrill erosion processes on steep loess hillslopes of China. *Soil and Tillage Research*, 184, 109-117. https://doi.org/10.1016/j.still.2018.07.007

875 Table 1: Information of each station considered in this study.

SC RANK	Station Name	Data Range	Upstream area (km^2)	Average Annual Load (kt)
1	Sakleshpur	2013-2017	617	32.46
2	M.H. Halli	1994-2017	3050	14.91
3	*Akkihebbal*	1994-2017	*5236*	23.18
4	Kudige	1974-2017	1934	124.59
5	Kollegal	1972-2017	21082	273.86
6	Muthankera	1974-2017	1260	165.81
7	T.Narasipur	1972-2017	7000	145.34
8	T.K. Halli	1985-2017	7890	38.31
9	T. Bekuppe	2013-2017	3500	11.34
10	Biligundulu	1972-2017	36682	834.86
11	Kudlur	2013-2017	709	2.35
12	Urachikottai	2001-2017	44100	50.10
13	Thengumarahada	2002-2017	1370	15.74
14	Nellithurai	2003-2017	1475	38.40
15	*Savandapur*	1980-2017	*5776*	24.25
16	Kodumudi	1973-2017	53233	331.41
17	Elunuthimangalam	2013-2016	3386	7.13
18	*Nallamaranpatty*	1980-2017	*9080*	43.17
19	*Musiri*	1973-2017	*66243*	519.84

876

877

878 Table 2: Description of the parameters and their distribution range

879

Parameters	Abbreviation	Minimum	Maximum	Mean	Std. deviation
Sediment yield	Y	2.05	131.85	41.35	47.92
Area (km^2)	A	592.31	8660.50	3143.16	2559.07
Perimeter (km)	P	148.61	545.59	321.06	138.91
Stream length (km)	SL	148.15	2316.02	823.29	675.42
Drainage density (km/km^2)	Dd	0.22	0.28	0.26	0.01
Basin length (km)	Bl	35.37	145.39	86.59	38.24
Mean elevation (m)	E	234.10	1267.08	756.46	318.52
Max Elevation (m)	Emax	1180.00	2629.00	1805.00	487.07
Min elevation (m)	Emin	82.00	899.00	447.00	284.68
Relief (m)	R	418.00	2394.00	1358.00	655.49
Relief ratio	Rr	5.95	43.88	18.49	12.47
Form factor	Ff	0.16	0.57	0.39	0.12
Circularity ratio	Rc	0.25	0.40	0.34	0.04
Elongation ratio	Re	0.15	0.20	0.18	0.01
Hypsometric Integral	HI	0.08	0.40	0.22	0.10
Slope (degree)	S	1.79	14.29	5.72	3.95
Slope-length factor	LS	1.19	18.36	6.22	5.13
Plan curvature	Cpln	0.002	0.01	0.008	0.005
Profile curvature	Cpro	0.002	0.01	0.008	0.005
Topographic ruggedness index	TRI	2.62	18.03	7.43	4.84
Topographic wetness index	TWI	7.47	10.02	8.83	0.93
Normalized steepness index	ksn	6.15	107.34	32.84	33.65
Lineament density (km/km^2)	Ld	0.13	2.85	0.89	0.74
Rainfall (mm)	Rain	661.13	2662.33	1253.38	671.46
Temperature (degree C)	Temp	19.93	28.10	24.01	2.48
Water area (%)	Watr	0.13	3.84	1.47	1.04
Tree area (%)	Tree	8.37	80.73	41.22	29.08
Crop area (%)	Crop	4.31	63.81	33.44	24.20
Built-up area (%)	Bilt	0.65	30.63	11.12	9.68
Rangeland area (%)	Rang	2.48	39.97	12.72	10.09

880

881

882 Table 3: PLSR model's explainability and quality for each component.

Index	Comp1	Comp2	Comp3	Comp4	Comp5
Q^2 cum	-0.245	-0.384	-1.794	-2.699	-4.825
R^2Y cum	0.286	0.419	0.551	0.714	0.801

883

884